FEDERAL STATE UNITARIAN ENTERPRISE
**“SCIENTIFIC RESEARCH INSTITUTE
SCIENTIFIC INDUSTRIAL ASSOCIATION “LUCH”
FSUE "SRI SIA "LUCH"**

APPROVED
General Director
I.I. Fedik

ANALYSIS OF MATERIAL STUDIES OF WWER-1000 MODEL ASSEMBLY TESTED AT THE PARAMETER-SF2 EXPERIMENT UNDER THE CONDITIONS OF SEVERE ACCIDENT WITH TOP AND BOTTOM FLOODING

Report
on scientific work
under ISTC Project No.3690

Project Manager
V.I. Nalivaev

Project Sub-Managers:
A.E. Kiselev
V.P. Semishkin

2008

Abstract

The studies were performed according to the Work Plan for ISTC Project No.3690 “Study of fuel assemblies under severe accident top quenching conditions in the PARAMETER-SF test series”.

The report presents the results of material studies of a 19-rod model assembly of WWER-1000 after the PARAMETER-SF2 experiment under the conditions of initial stage of severe accident with the combined top and bottom quenching of FA overheated to 1500°C.

The objective of material studies was a description of the post-test state of the model assembly and analysis of its components (structure, oxidation, fragmentation).

The studies included the following:

- encapsulation and sectioning of the model FA;
- preparation of cross section slabs;
- optical and electronic microscopy;
- X-ray analysis;
- analysis of the obtained results.

The report includes 45 pages, 2 Tables, 33 Figures.

CONTENTS

INTRODUCTION

SF2 experiment was performed with the aim of studying the behaviour of a 19-rod model FA of WWER-1000 under simulated severe accident conditions. In the experiment the initial stage of severe accident was simulated with large coolant leak from the primary circuit of WWER-1000 RP when the core drying occurs as well as its heating-up to ~ 1500°C and top and bottom water quenching.

The main purposes of the experiment were:

- Study of behaviour of structural components of a 19-rod model FA of WWER-1000 (fuel pellets and claddings, shroud, spacer grids);
- Study of temperature evolution of cooling a 19-rod model FA of WWER-1000 overheated to ~ 1500°C with top and bottom quenching;
- Study of oxidation degree of structural components of a 19-rod model FA of WWER-1000;
- Study of interaction and structural-phase changes in the materials of a model FA of WWER-1000 (fuel pellets and claddings);
- Study of hydrogen release.

General purposes of the experiment governed the aims and tasks of material studies and namely:

- description of state of the model FA structural components;

- determination of thicknesses of oxide layers of fuel rod claddings and their distribution over FA height;

- quantitative evaluation of total hydrogen mass generated by the end of the experiment on the basis of the results of material studies.

Material studies were performed according to the Work Plan for ISTC Project No.3690 “Study of fuel assemblies under severe accident top quenching conditions in the PARAMETER-SF test series”.

1. METHODS OF MATERIAL STUDIES

1.1. Methods of encapsulation and sectioning of the model FA

After the experiment the test section was disassembled and the state of model FA inside the test section was fixated with a compound (epoxy resin ЭД-20) in vertical position.

After the compound hardened, the assembly was removed from the test section, photographed in detail and cut over the height into slabs. Sectioning of the bundle was done with the use of cutting-off machine Delta-Abrasimet with diamond blade of thickness 1.7 mm. Thickness of cross section slabs was chosen to be 15…20 mm to be ensured in their integrity keeping during their cutting out (to avoid their transverse cracking and spilling out of FA components). The elevations of the cross section are presented in Table 1. The elevations were determined according to the methods of material studies described below.

To remove voids and cavities remained after FA filling with the compound the cross section slabs vacuum impregnation was made with epoxy resin EPO – THIN at the “Buehler” impregnator. Then the cross section slabs have been ground and polished.

The macro photos of the ground cross section slabs were taken by the digital camera SONY (8 mps) (Fig. 2. 3). Further on, the available macrographs were used for comparative evaluation of the degree of the assembly damage at different elevations.

1.2. Methods of material studies of the model FA

Methodical approaches to material studies of the assembly are developed on the basis of the analysis of results of measurement of fuel rod cladding temperature (see Fig. 1 a) in the PARAMETER-SF2 experiment, [1]. The highest temperatures in the assembly were reached on claddings of fuel rods of the second row. Fig. 1 b presents temperature distribution over the bundle height for the 2^{nd} row claddings restored by the method of interpolation by indications of thermocouples, at the beginning of pre-oxidation stage (moment t=12000 s), at the beginning of the transient stage (moment t=15300 s), and directly before the filling (moment t=16500 s). Temperature points at the elevations correspond to thermocouples indications at the corresponding time moments.

In the lower part of heated zone (0 – 400 mm) the relatively low temperatures (as to the oxidation process) were recorded. Maximum temperature in the lower part (0 – 400 mm) in the course of the experiment did not exceed ~ 850°C (Fig. 1 b). Basing on the oxidation kinetics of alloy E110, [2, 3], one should expect the low oxidation degrees in this area. Results of check studies of the oxidation degree of fuel rods and shroud in this area

confirmed the given conclusion. Thickness of oxide layer on claddings and shroud at the elevation of Z = 400 mm is not high and corresponds to be ~ 5…10 μm.

The main attention in post-test studies was directed to the FA middle (500 – 800 mm) and upper (900 – 1300 mm) parts. For metallographic studies 11 cross section slabs were prepared from these elevations.

In the middle part (500 – 800 mm) of the assembly the maximum temperatures of the 2nd row fuel rods did not exceed 1170°C (Fig. 1 b). Thermocouples show the pre-oxidation of claddings of the fuel rods of the 2nd row occurred at temperatures 800-950°C. According to the data of [2, 3, 4], the alloy E110 show breakaway at temperature below 1100°C and long-term exposure. Therefore in this area of the assembly one should expect the dioxide of layered structure with trend to separate from the cladding. Information on the state of the assembly components in this area can be also used for understanding of intermediate states of the assembly components located at higher elevations. For metallographic measurements of thickness of oxide and metal layers on cladding surfaces four cross section slabs were chosen at 513, 605, 702 and 769 mm elevations (Table 1, Fig. 2). Description of the state of the assembly components in this area was performed for 513 mm and 702 mm elevations.

According to the thermocouple readings, the hottest zone location corresponds to the assembly upper part at 900…1300 mm elevations (Fig. 1 b). So, in this part of the assembly, one should expect the highest degree of oxidation of the shroud and claddings. Therefore, the metallographic measurements of layers thickness in this area were done with more detail (for the elevations of 902, 951, 1033, 1103, 1203, 1246 and 1296 mm, Table 1, Figs. 2, 3). High temperature (at pre-oxidation and transient phases) allows expecting under external layered oxide compact oxide well connected with metallic layer.

Description of the state of the assembly components in this area was made for the following cross section slabs:

Z = 1033 mm – the area of location of the intact spacer grid and the most long-term cooling, [1];

Z = 1103 mm – the area of finding of local fragmentation of fuel rod claddings;

Z = 1246 mm – the hottest area of the assembly in the course of the experiment.

For all cross section slabs chosen (Table 1) the thickness of metal layers and dense oxide of fuel rod claddings were measured. The necessity of measurement of metal layer thickness was caused by the morphology of oxide scale – at the most elevations the cladding surface has both the compact oxide, and the easily spalled off

oxide of layered structure, that does not allow the accurate measurement of the zirconium dioxide scale.

The measurements were done, if possible, on each cladding in four directions around rods and for all selected and chosen cross section slabs and averaged. By the results of measurements curves of distribution of thicknesses of metal part of claddings and of compact dioxide over the assembly heated zone were plotted The calculated claddings oxide scale thicknesses defined as a difference between the original tube wall thickness to be 690 μm and the thickness of metal part remained (considering Pilling-Bedworth factor) are presented as well.

Metallographic analysis of cross section slabs was performed with the optical microscope OLYMPUS using the computer code package OMNIMET. Electron microscope studies of cross-sections were performed with the scanning electron microscope JEOL JSM – 6460 LV.

X-ray studies of the assembly zirconium structural components were performed on specimens cut out of the shroud (Z ~ 250, 500, 900 and 1200 mm, specimen size – 15x20 mm). We did not manage to prepare similar specimens of claddings because any attempt to withdraw claddings from cross section slabs resulted in cladding damage.

Phase analysis of specimens by X-ray was performed on the external shroud surface (because the concavity of the inside surface does not allow performing the analysis in the inside), as well as at a depth of 30 and 200 μm from the external surface and in the middle of the shroud thickness (~1000 μm). At 900 mm elevation, where the maximum hydrogen content was found, the additional studies were performed at the depth of 1300, 1400, 1500 and 1600 μm. Material layers were removed by etching in the mixture of hydrogen peroxide, nitrogen and hydrofluoric acids. Thickness of the etched layers was measured with micrometer.

X-ray of specimens was performed with the diffractometer DRON-6 basing on Cu$K\alpha$ – radiation. The mode of photography in performing the qualitative phase analysis was chosen to be such that the ratio of diffraction lines of β - and ω - phases would be maximum. Difficulty of interpretation of diffraction spectra of specimens was due to the fact that on the front diffraction angles the reflections of hexagonal ω - phase are superimposed on the reflections of phase β - Zr, therefore the presence of ω - phase was revealed, first of all, by appearance of line (112) at an angle of $2\theta \approx 71$ deg.

The amount of ZrH_2 phase was measured by ratio of integral intensities of analytical lines. Line (111) – the most intensive in the diffraction spectrum of ZrH_2, was used as the analytical line. Measurements were performed in each studied section in layer-by-layer

radiography phase analysis. With this, it was considered that in the course of tests the grain sizes of α-solid solution of zirconium could increase to 200 μm and more as a result of recrystallization. Due to large grain size the statistical distribution of orientations, necessary for normal ratio of intensities, is not reached. Besides, in the shroud materials there may be texture and the quantitative ratios of phases may change by its section. All these facts could make considerable changes in the ratio of intensity-concentration and, as a consequence, introduce an uncertainty into the results of X-ray phase analysis of the compact shroud sections. The most suitable specimens for performing the quantitative X-ray phase analyses are powders. Owing to this, at the elevations (Z ~ 250, 500, 900 and 1200 mm) measurements of ZrH_2 phase content were performed also on powder samples got by means of filing the shroud fragments by diamond needle file from the outside surface by the depth of not more than a half of the shroud thickness. Lattice periods of β - and ω - phases were determined with an error of ±0.01 Å.

Accuracy of determination of a and c periods of α-solid solution depended on the width of diffraction lines, i.e. on the degree of the lattice distortion. In the most favourable cases an error in determination of a and c periods did not exceed ±0.001 Å.

2. RESULTS OF MATERIAL STUDIES

2.1. Description of the shroud posttest appearance

Visual examination of the model FA shroud after removing of the encapsulated assembly from the test section showed that its external surface is covered with firm black zirconium oxide (Fig. 4), and its post-test integrity is fully kept (no blowholes, deformation and cracks).

However in the course of the assembly sectioning into slabs (when it is chucked in Delta-Abrasimet machine) the shroud brittle crack occurred over the generatrix (opposite fuel rod 3.4), that is indicative of a considerable saturation of metal with oxygen and possible formation of zirconium hydrides.

2.2. Structural analysis of cross-sections

2.2.1. Elevations of 500 – 900 mm

At Z = 513 mm elevation (top view, location of spacer grid (SG) No. 4) there are practically no visible damages of the assembly (Fig. 5). Maximum temperature of claddings at this elevation at the pre-oxidation stage did not exceed ~ 820°C, and before flooding onset ~ 950°C (Fig. 1). There are cracks on some pellets of uranium dioxide. In some pellet there are no fuel fragments. However crumbling of pellets occurred probably in the course of the assembly sectioning or following preparation of cross section slabs for metallographic examinations.

Oxidation of zirconium structural components (fuel rod claddings, shroud and spacer grid) at this elevation in steam environment resulted in formation of multi-layerd spalled off oxide scale on their surfaces (Fig. 6). At the places of contact of fuel rod simulator 1.1 with the spacer grid there was stronger oxidation of the cladding (Fig. 7 b). The cladding metal layer thickness was found to be ~ 600 μm, for other fuel rods, to be ~ 650 μm. Also in the given section the fragments of fuel rod claddings, grids and oxide films were found in the spacer grid cells that, evidently, fell down from higher elevations.

Structural state of claddings at the given elevation is characterized by the following:

- calculated thickness of oxide scale on the cladding external surfaces is 20… 110 μm;

- thickness of zirconium oxide, well connected with metallic substrate, varies within the range of 7…20 μm.

The remained metal part of claddings consists of two layers: α - Zr(O), with thickness of not more than 30 μm. and β - Zr. Values of metal layer thickness in the cross section vary from ~ 610 to 670 μm.

Results of measurements of thickness of the remained metal part of claddings at Z = 513 mm elevation are shown in Fig. 8. Calculated values of oxide layers – in Fig. 33.

At Z = 702 mm elevation (top view) the cross-section geometry changed insignificantly (the displacement of fuel rod 1.1 in respect to its initial position is observed, Fig. 9). Maximum cladding temperatures at this elevation at the pre-oxidation stage did not exceed ~ 970°C, and before flooding onset~ 1100°C (Fig. 1). A considerable difference is revealed in the oxidation degree between the central fuel rod (fuel rod 1.1) and the other fuel rods, namely the cladding of fuel rod 1.1 is oxidized considerably stronger (Fig. 10), on its surface there is a thick multilayered oxide scale (Fig. 11 a, c), whereas the other simulators are covered with the oxide consisting of only a few or several layers. On all fuel rods the essential spallation of oxide from the surface of fuel rod claddings is observed (Fig. 11 b, d). No fuel-clad interaction, internal claddings oxidation and through wall cracks are revealed in claddings. Thickness of metal part of claddings varies from 630 to 660 μm, in the central fuel rod 1.1 – 510 μm.

Structural state of claddings at the given elevation is characterized by the following:

- calculated thickness of oxide scale on the cladding external surfaces is 30… 110 μm, in the central fuel rod 1.1 – 270 μm;

- thickness of zirconium oxide well connected with metallic substrate, varies within the range of 15…20 μm.

The remained metal part of claddings consists of two layers: α - Zr(O), with thickness of not more than 50 μm, and β - Zr. Thickness of cladding metal part varies from 630 to 660 μm, in the central fuel rod 1.1 – 510 μm.

Generalized results of measurements of thickness of the remained metal part of claddings for different fuel rods at Z = 702 mm elevation are presented in Fig. 12. Calculated values of oxide layers are given in Fig. 33.

2.2.2. Elevation interval of 900 – 1300 mm

At Z = 1033 mm elevation (top view, arrangement of SG No.2) the considerably higher degree of oxidation of fuel rod simulators is observed as compared to the described lower elevations (Fig. 13). Maximum cladding temperatures at this elevation at the pre-oxidation stage did not exceed ~ 1150°C, and before flooding ~ 1370°C (Fig. 1). It should be noted that approximately in this area the long-term assembly cooling took place, however it did not influence principally the cladding structures. Typical state of fuel rod simulators is shown in Fig. 14. On their surface there is an easily spalled off oxide ZrO_2, under which the layer of compact, zirconium oxide with columnar microstructure well

connected with metal substrate, is located (Fig. 15). In the layer α - Zr(O) there are numerous radial cracks penetrating the β - phase. Edges of these cracks are not oxidized (Fig. 17). Many of fuel rods (2.1, 2.3, 2.4, 2.5, 2.6, 3.1, 3.2, 3.3, 3.4, 3.5, 3.6 and 3.12) have the through wall cracks, however no cladding fragmentation, fuel relocation and fuel-clad interaction are revealed. Internal oxidation in some fuel rod claddings was found but it is insignificant. In oxidation of fuel rod 2.5 (Fig. 15 b) there is a peculiarity of formation of considerably thicker spalled off oxide scale as compared to other fuel rods (Fig. 15 a, c). With this, the thickness of compact oxide for fuel rod 2.5 to be ~ 180 μm is in a good agreement with other fuel rods (Fig. 31).

In the spacer grid cells there is a considerable number of fragments of oxide scales. The cells themselves also have the through wall cracks (Fig. 16) and is oxidized completely (for the second row of fuel rods).

Structural state of claddings at the given elevation is characterized by the following:

- calculated thickness of oxide scale on the cladding external surfaces is 120…300 μm, in fuel rod 2.5 – 580 μm;

- thickness of compact zirconium dioxide with columnar structure varies within 100…200 μm.

The remained metal part of claddings consists of two layers: α - Zr(O), with thickness of not more than 300 μm, and β - Zr. Thickness of metal part of claddings varies from 490 to 600 μm, in fuel rod 2.5 – 310 μm.

Results of measurements of thickness of the remained metal part of claddings at Z = 1033 mm elevation are shown in Fig. 18. Calculated values of oxide scale - in Fig. 33.

At Z = 1103 mm elevation (top view) further increase in the oxidation degree of fuel rod simulators and their displacements relative to the initial positions are observed (Fig. 19). Maximum cladding temperatures at this elevation at the pre-oxidation stage did not exceed ~ 1180°C, and before flooding onset – ~ 1400°C (Fig. 1). Typical state of fuel rod simulators is shown in Fig. 20. On their surface there is also an easily spalled off oxide ZrO_2, under which the layer of compact, zirconium dioxide with columnar structure well attached to metal substrate is located (Fig. 21). It should be pointed out that compact oxide tends to split (Fig. 21 a). Owing to brittleness of suboxide layer all fuel rods practically have a large number of non-oxidized cracks (Fig. 22), and some of the fuel rods (fuel rods 2.1, 2.3 and 3.2) are fragmented. However no fuel crumbling and fuel-clad interaction are revealed also.

There is internal oxidation in some fuel rod claddings, with this, oxide layer thickness reaches ~ 20…50 μm. At the given elevation there is a peculiarity in oxidation of fuel rod 2.2 (Fig. 21 b), similar to oxidation of fuel rod 2.5 at Z = 1033 mm elevation.

Structural state of claddings at the given elevation is characterized by the following:

- calculated thickness of oxide scale on the cladding external surfaces is 120… 420 μm, in fuel rod 2.2 – 580 μm;

- thickness of a compact zirconium dioxide with columnar structure varies within 100…200 μm.

The remained metal part of claddings consists of two layers: α - Zr(O), with thickness of not more than 400 μm, and β - Zr. Thickness of metal part of claddings varies from 410 to 600 μm, in fuel rod 2.2 – 308 μm.

Results of measurements of thickness of the remained metal part of claddings at Z = 1103 mm elevation are presented in Fig. 23. Calculated values of oxide layers – in Fig. 33.

At Z = 1246 mm elevation (top view) the rods arrangement is distorted significantly (Fig. 24). This is hottest zone of the assembly. Maximum cladding temperatures at this elevation at the pre-oxidation stage did not exceed ~ 1250°C, and before flooding onset ~ 1500°C (Fig. 1). Typical state of fuel rod simulators is shown in Fig. 25. The fuel rod claddings have the through wall cracks, but they are not fragmented.

Cladding oxide scale has multilayered structure. Earlier grown oxide ZrO_2 with fine structure (Fig. 26), namely the layered sequence of very thin films, tends to interior spallation. Internal part of this dioxide either is detached from younger compact dioxide or tends to detach. Internal compact layer was found split in azimuthal direction for many rods and external split part is detached from internal one (Fig. 26).

Metal part of claddings presents itself an oxygen-stabilized α - phase (α - Zr(O)), and a great number of cracks is indicative of its brittleness. There is internal oxidation in some fuel rod claddings, with this, the oxide layer thickness reaches ~ 30…50 μm. At the given elevation no fuel relocation and fuel-clad interaction are revealed also. Crack edges in some fuel rods are oxidized (Fig. 27).

Structural state of claddings in the hottest zone of the SF2 assembly is characterized by the following:

- calculated thickness of the oxide scale on the cladding external surfaces is 300…650 μm;

- thickness of the compact columnar zirconium oxide well connected with the α - Zr(O) layer varies within 100…350 μm.

The remained metal part of claddings presents itself the phase α - Zr(O), radial distribution of metal layer thickness is considerably nonhomogeneous, the values vary from 250 to 500 μm.

Results of measurements of thickness of the remained metal part of claddings at Z = 1246 mm elevation are presented in Fig. 28. Calculated values of oxide layers – in Fig. 33.

2.3. Distribution of fuel rod cladding oxidation over heated zone

In studying the assembly cross-sections it was revealed that within the elevation of 500 – 1300 mm the oxide scale on the cladding external surfaces has the layered structure, the external oxide layers are spalled off, there is a partial loss of a part of zirconium dioxide layer on the cladding surface in the course of oxidation, flooding and during preparation of cross section slubs. In this situation the direct measurements of the zirconium dioxide layer thickness will result in significant errors. A possible method for evaluation of the oxide scale thickness is the method of calculation using the data of metallographic measurements of thickness of the remained metallic part of claddings. Evaluation of the split off fraction in the oxide scale (spalled off layers due to breakaway effect and split off part of compact oxide due to its cracking) is possible on the basis of thickness of the compact zirconium dioxide attached to metallic substrate that can be also measured by metallographic method.

Thicknesses of the compact oxide and the remained metal part of claddings were measured on each fuel rod and, as a minimum, in four azimuthal directions, if possible (because in some cases claddings fragmentation was observed). Results of these measurements are presented in the form of plots (Fig. 29 - 32), and for the convenient analysis –for the second and the third row separately.

Analysis of the results of measurements showed that:

- within the elevation of 500 – 900 mm the thickness of metal part of claddings of the fuel rods of the second and third rows is practically constant and equal to ~ 650 μm. The exception is the fuel rod 1.1 oxidized considerably stronger (there were no pellets);

- then, up to ~1250 mm elevation (the hottest area), the metal layer thickness for claddings both in the second and third rows reduces monotonously from ~ 500 to ~ 250 μm. The exception is the fuel rods 2.5 (Z = 1033 mm) and 2.2 (Z = 1103 mm). Their strong oxidation occurred, evidently, at the temperatures within breakaway regime because the compact oxide thickness (the sign of high temperature oxidation) at the given elevations corresponds to the other fuel rods (Fig. 31). The larger scatter is observed both in thicknesses of metal part, and in thicknesses of compact oxide for claddings of the fuel rods of the third row;

- at unheated part (Z ~1300 mm) the oxidation degree of claddings in the second and third rows reduces somewhat.

2.4. Results of X-ray analysis of the assembly elements

The analysis was made for the shroud specimens in the original state and for the shroud after the tests from 250, 500, 900 and 1200 mm elevations. Results of phase analysis of the shroud specimens are given in Table 2.

The shroud material in the original state consisted of two phases - solid solutions based on α- Zr and β-Nb. After the tests the material phase composition at different assembly elevations was different. Within the elevation of Z = 500… 1200 mm there was the phase of zirconium oxicarbide ($Zr(C_xO_{1-x})$) with the lattice period a = (4.67±0.01)Å. Origination of this phase is caused, evidently, by insufficient degassing of thermal insulation before the experiment. Starting from Z = 250 mm elevation and abover a thin film of ZrO_2 of monoclinic modification was found on the shroud external surface.

Change of the lattice periods of α-solid solution, as compared to the original state, is caused by dissolution of gas impurities (O, H) in it and by redistribution of alloying element (Nb) between the phase components of material in the course of heating-up and flooding the assembly.

Alongside with α - Zr and δ - ZrH_2, depending on the elevation, there were β - (Zr, Nb) – solid solutions and metastable ω - phase (Z ~ 500 mm) in the shroud material.

Zirconium hydride ZrH_2 in the shroud material was revealed at 500, 900 and 1200 mm elevations. Through the shroud thickness, from the outside surface into the depth, the decrease of hydride phase content is observed. The maximum value of ZrH_2 content to be 22% vol. (hydrogen content – 24% at.) was revealed at Z ~ 900 mm elevation.

It should be noted that in the given work the method of X-ray analysis allows measurements of content of hydrogen presented only in the condensed phase (i.e. zirconium hydride). On the basis of these data the hydrogen mass in the remained metal part of the shroud can be evaluated to be ~ 2 g.

2.5. Evaluation of hydrogen mass

The maximum hydrogen amount that could be generated by the end of the SF2 experiment, can be evaluated on the basis of the metallographic and X-ray data on the claddings oxide layers thickness and hydrogen content in the shroud.

Oxidation of the following assembly components and measurement systems elements was taken into account (they are listed in accordance with their contribution into the total hydrogen mass):

1) the fuel rod claddings at Z = 400…1500 mm elevations;

2) the shroud at Z = 400…1500 mm elevations;

3) the zirconium sheath of thermocouples and pressure sensors, [1];

4) the spacer grids (Nos.1 and 2);

5) the fuel UO_2, tantalum heaters, molybdenum electrodes, thermocouples cables, structural components of the test section at the upper part.

The amount of hydrogen, that could be generated due to oxidation of fuel rod claddings, was evaluated by the oxygen mass in α - Zr(O) and ZrO_2 layers. With this, it was assumed that the zirconium dioxide layer is stoichiometric, oxygen content in α - Zr(O) was assumed to be 20% at.

Within the elevations of Z = 950…1500 mm no β - phase remains practically due to strong oxidation, therefore the thickness of layer α - Zr (O) was assumed equal to the thickness of metal part. Within the elevations of Z = 400…950 mm the cladding metal part presents itself the layers of β - phase and the layer of α - phase. Presence of typical irregular “sawlike” boundary of α - Zr (O) layer in alloy E110 results in the fact that it is impossible to define the geometrical boundary between α - Zr (O) and β phases. So the thickness of α - Zr (O) layer was estimated with the accuracy of 10…20 μm. The oxygen content in the claddings below 400 mm may be neglected due to small thickness of oxide layer.

Considering the given assumptions the estimated hydrogen mass from claddings oxidation does not exceed ~ 20 g. Estimated hydrogen mass from the shroud oxidation does not exceed ~ 7 g (considering its less surface area).

According to the estimations, the oxidation of zirconium thermocouples sheath and pressure sensors could contribute not more than ~ 2 g of hydrogen because their surface area is less than 10% of surface area of fuel rods.

During the experiment, the SGs No.1 and No.2 were oxidized practically completely. Hydrogen release due to the spacer grids oxidation can be assess to be ~ 2 g if we assume that the whole amount of zirconium is transformed into stoichiometric oxide.

The studies of fuel structure, heaters, current leads, thermocouples electrodes as well as evaluation of temperature of the test section upper part showed that hydrogen generation caused by the above-mentioned components oxidation is insignificant and may be neglected.

So, the total hydrogen amount that could be generated due to assembly materials oxidation does not exceed ~ 31 g. With this, it should be noted that a portion of hydrogen,

generated in the course of the experiment, diffused into the cladding, remained in metal phase of zirconium in the form of solid solution and hydride phase, and its amount did not determined exactly.

CONCLUSIONS

Analysis of post-test material studies showed that the assembly axial temperature profile led to different degree of its damages.

The state of the lower part of heated zone (Z = 0…400 mm) does not practically differ from the original state, and oxide thickness on the external surface does not exceed 5…10 μm.

At 500…1300 mm elevations there is a multilayered spalled off zirconium dioxide. Comparison of the results of metallographic studies and thermocouples indications allow supposing that pronounced breakaway oxidation over such an extended zone would occurred during the pre-oxidation. phase.

In the middle part of heated zone (Z = 500…800 mm) the fuel rod simulators are displaced relative to the original arrangment, the external claddings surface is covered with multilayered zirconium dioxide, separating from metal surface, but its thickness does not exceed ~ 100 μm.

In the upper part of heated zone (Z = 900…1300 mm) the original arrangement is greatly distorted. The claddings are oxidized both on the external (to 650 μm), and on the internal (to 50 μm) surfaces. Zirconium dioxide has different morphology. The internal part of the oxide scale is a compact, well-connected with the metal layer, zirconium dioxide that was grown, evidently at the transient stage. In the hottest sport compact dioxide cracked in azimuth direction with trend to split off. One can suppose that this effect resulted from thermoshock during top flooding. Thickness of compact zirconium dioxide attached to metal layer increases with elevation increase and reaches the maximum value at the elevations of 1250-1300 mm, and distribution of its thickness through the assembly section at the given elevations is signifinantly nonhomogeneous and varies within the range of 100…350 μm.

Outside the compact dioxide there is the zirconium dioxide of multilayered structure, separating from inner dioxide. The metal part of the claddings presents the oxygen-stabilized α phase (α - Zr (O)). The fuel rod claddings are embrittled, i.e. have through wall cracks, however fragmentation of fuel rods is limited. No fuel relacation and fuel-clad interaction are revealed in the assembly.

On the basis of the results of metallographic studies the evaluation was done for the maximum possible hydrogen mass that could release into steam-gas environment during the experiment. Taking into account the results of measurement of hydrogen content in the shroud, the upper limits of total hydrogen mass in the steam-gas environment can be

estimated to be 31 g. The assessed value is in a good agreement with the results of measurements (~ 28 g).

References

1. Protocol of PARAMETER-SF2 Experiment Results (April 3, 2007), p. 51.
2. Bibilashvili Yu.K., Sokolov N.B., Andreyeva-Andrievskaya L.N., Salatov A.V., Morozov A.M. “High-Temperature Interaction of Fuel Rod Cladding Material (Zr1%Nb Alloy) with Oxygen-Containing Medium”, IAEA-TECDOC-921, Dimitrovgrad, 1995.
3. В.И.Соляный, Ю.К.Бибилашвили, В.В.Драненко, Л.Б.Израилевский, А.Я.Левин, А.М.Морозов. «Исследования коррозионного поведения оболочек твэлов из сплава Zr-1%Nb в паре при высоких температурах», Вопросы атомной науки и техники, серия: Атомное материаловедение, 1988. вып.2(27), 89-95.
4. M. Steinbruck, J. Birchley, A.V. Goryachev, M. Grosse, T. J. Haste, Z. Hozer, A.E. Kisselev, V.I. Nalivaev, V.P. Semishkin, L. Sepold, J. Stuckert, N. Ver, M.S. Veshchunov, “Status of studies on high-temperature oxidation and quench behaviour of Zircaloy-4 and E110 cladding alloys”, The Third European Review Meeting on Severe Accident Research, 23-25 September 2008 Nesseber, Bulgaria.

Appendix

Table 1

Cross sections for metallographic examination of the SF2 bundle

Specimen	Specimen length, mm	Specimen coordinate		Remarks
		Bottom, mm	Top, mm	
	380	0	380	
Cut	1.7	380	381.7	
	18	381.7	399.7	Polished
Cut	1.7	399.7	401.4	
	49	401.4	450.4	
Cut	1.7	450.4	452.1	
	41	452.1	493.1	
Cut	1.7	493.1	494.8	
	18	494.8	512.8	Polished
Cut	1.7	512.8	514.5	
	19	514.5	533.5	
Cut	1.7	533.5	535.2	
	50	535.2	585.2	
Cut	1.7	585.2	586.9	
	18	586.9	604.9	Polished
Cut	1.7	604.9	606.6	
	75	606.6	681.6	
Cut	1.7	681.6	683.3	
	19	683.3	702.3	Polished
Cut	1.7	702.3	704	
	45	704	749	
Cut	1.7	749	750.7	
	18	750.7	768.7	Polished
Cut	1.7	768.7	770.4	
	18	770.4	788.4	
Cut	1.7	788.4	790.1	
	60	790.1	850.1	
Cut	1.7	850.1	851.8	

	33	851.8	884.8	
Cut	1.7	884.8	886.5	
	15	886.5	901.5	Polished
Cut	1.7	901.5	903.2	
	29	903.2	932.2	
Cut	1.7	932.2	933.9	
	17	933.9	950.9	Polished
Cut	1.7	950.9	952.6	
	65	952.6	1017.6	
Cut	1.7	1017.6	1019.3	
	14	1019.3	1033.3	Polished
Cut	1.7	1033.3	1035	
	17	1035	1052	
Cut	1.7	1052	1053.7	
	30	1053.7	1083.7	
Cut	1.7	1083.7	1085.4	
	18	1085.4	1103.4	Polished
Cut	1.7	1103.4	1105.1	
	51	1105.1	1156.1	
Cut	1.7	1156.1	1157.8	
	26	1157.8	1183.8	
Cut	1.7	1183.8	1185.5	
	17	1185.5	1202.5	Polished
Cut	1.6	1202.5	1204.1	
	21	1204.1	1225.1	
Cut	1.7	1225.1	1226.8	
	19	1226.8	1245.8	Polished
Cut	1.7	1245.8	1247.5	
	30	1247.5	1277.5	
Cut	1.7	1277.5	1279.2	
	17	1279.2	1296.2	Polished
Cut	1.7	1296.2	1297.9	
	50	1297.9	1347.9	

Table 2

Results of phase analysis by X-ray

Assembly coordinate, mm	Thickness of etched layer, μm	Phase composition	Lattice periods, a Å		Results of layer-by-layer analysis Content of H, % at.	Results of analysis of powder samples * Content of H, % at.
Shroud originall state	-	α - Zr + β - Nb	α - Zr	a = 3.229, c = 5.144	-	-
			β - Nb	3.548		
250 mm	0 (eternal surface)	α - Zr(O) + ZrO_2 monoclinic	α - Zr	a = 3.230, c = 5.149	-	-
	20	α - Zr + β - Nb	α - Zr	a = 3.231, c = 5.148	-	-
			β - Nb	3.34		
	300	α - Zr + β - Nb	α - Zr	a = 3.230, c = 5.148	-	-
			β - Nb	3.34		
	middle section	α - Zr + β - Nb	α - Zr	a = 3.230, c = 5.148	-	-
			β - Nb	3.34		
500	0 (external surface)	$Zr(C_xO_{1-x})$ + α - Zr	$Zr(C_xO_{1-x})$	4.66	-	9
			α - Zr	a = 3.249, c = 5.178		
	20	α - Zr + β - Zr + ω - Zr + δ-ZrH_2	α - Zr	a = 3.239, c = 5.164	10	
			β - Zr	3.56		
			ω - Zr	a = 5.02, c = 3.10		
			δ-ZrH_2	4.75		
	300	α - Zr + β - Zr + δ-ZrH_2+ ω - Zr(traces)	α - Zr	a = 3.235, c = 5.152	8	
			β - Zr	3.56		
			δ-ZrH_2	4.75		
	middle section	α - Zr + δ-ZrH_2+ β - Zr	α - Zr	a = 3.235, c = 5.161	6	
			β - Zr	3.55		
			δ-ZrH_2	4.75		
900	0 (external surface)	Zr(CO) + α - Zr	Zr(CO)	4.67	-	23
			α - Zr	a = 3.227, c = 5.150		

	20	α - Zr + δ-ZrH_2	α - Zr	a = 3.225, c = 5.147	24	
			δ-ZrH_2	4.77		
	300	α - Zr + δ-ZrH_2	α - Zr	a = 3.225, c = 5.145	21	
			δ-ZrH_2	4.77		
	1000	α - Zr + δ-ZrH_2	α - Zr	a = 3.224, c = 5.150	20	
			δ-ZrH_2	4.77		
	1300	α - Zr + δ-ZrH_2			17	
	1400	α - Zr + δ-ZrH_2			17	
	1500	α - Zr + δ-ZrH_2			17	
	1600	α - Zr + δ-ZrH_2			16	
1200	0 (external surface)	Zr(CO) + α - Zr	Zr(CO)	4.67	-	18
			α - Zr	a = 3.236, c = 5.178		
	20	α - Zr+ δ-ZrH_2 + β - Zr + β - Nb	α - Zr	a = 3.225, c = 5.150	21	
			δ-ZrH_2	4.76		
			β - Zr	3.56		
			β - Nb	3.33		
	300	α - Zr + δ-ZrH_2 + β - Zr + β - Nb	α - Zr	a = 3.229, c = 5.153	20	
			δ-ZrH_2	4.77		
			β - Zr	3.56		
			β - Nb	3.34		
	middle section	α - Zr + δ-ZrH_2 + β - Zr + β - Nb	α - Zr	a = 3.229, c = 5.178	18	
			δ-ZrH_2	4.77		
			β - Zr	3.57		
			β - Nb	3.34		

* - content of ZrH_2 phase was measured on powder samples got by filing the shroud fragments with diamond needle file from the external surface to the depth of not more than half of the shroud.

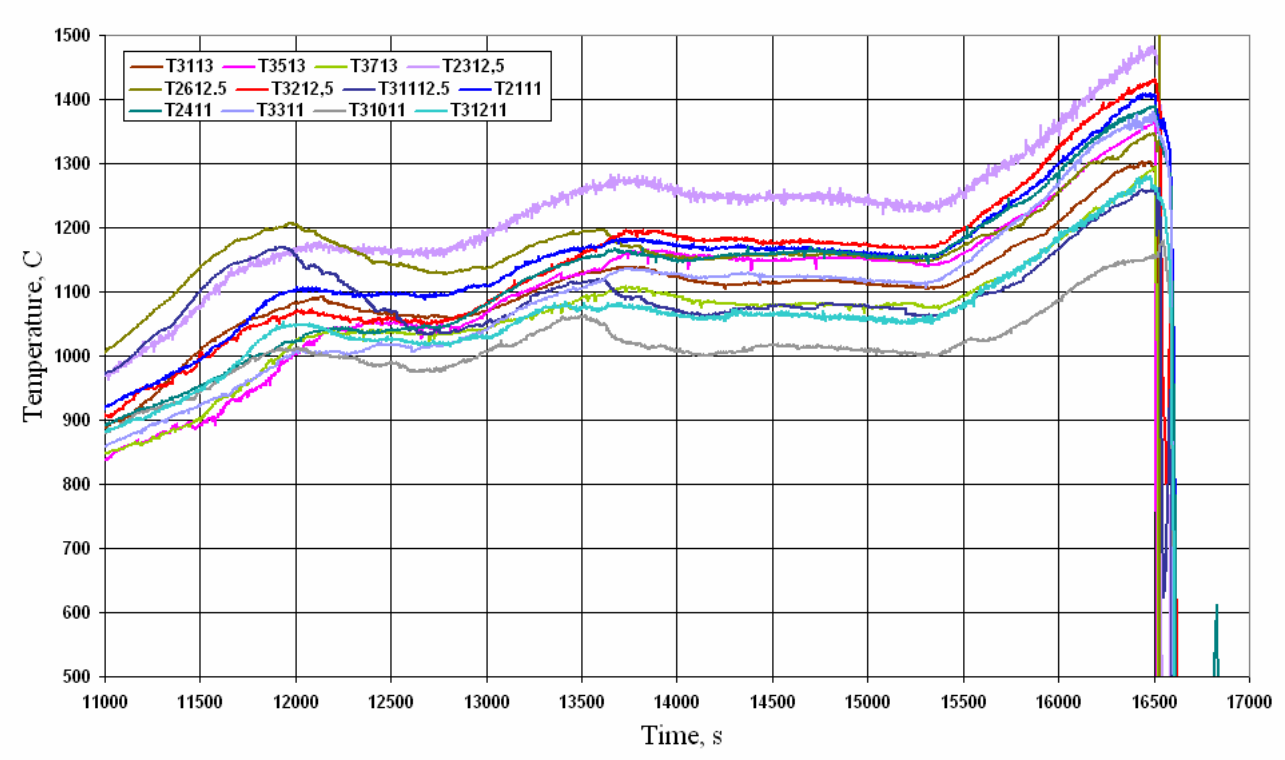
T3113
T3513
T3713
T2312,5
T2612.5
T3212,5
T31112.5
T2111
T2411
T3311
T31011
T31211
Temperature, C
Time, s
1500
1400
1300
1200
1100
1000
900
800
700
600
500
11000
11500
12000
12500
13000
13500
14000
14500
15000
15500
16000
16500
17000

a)

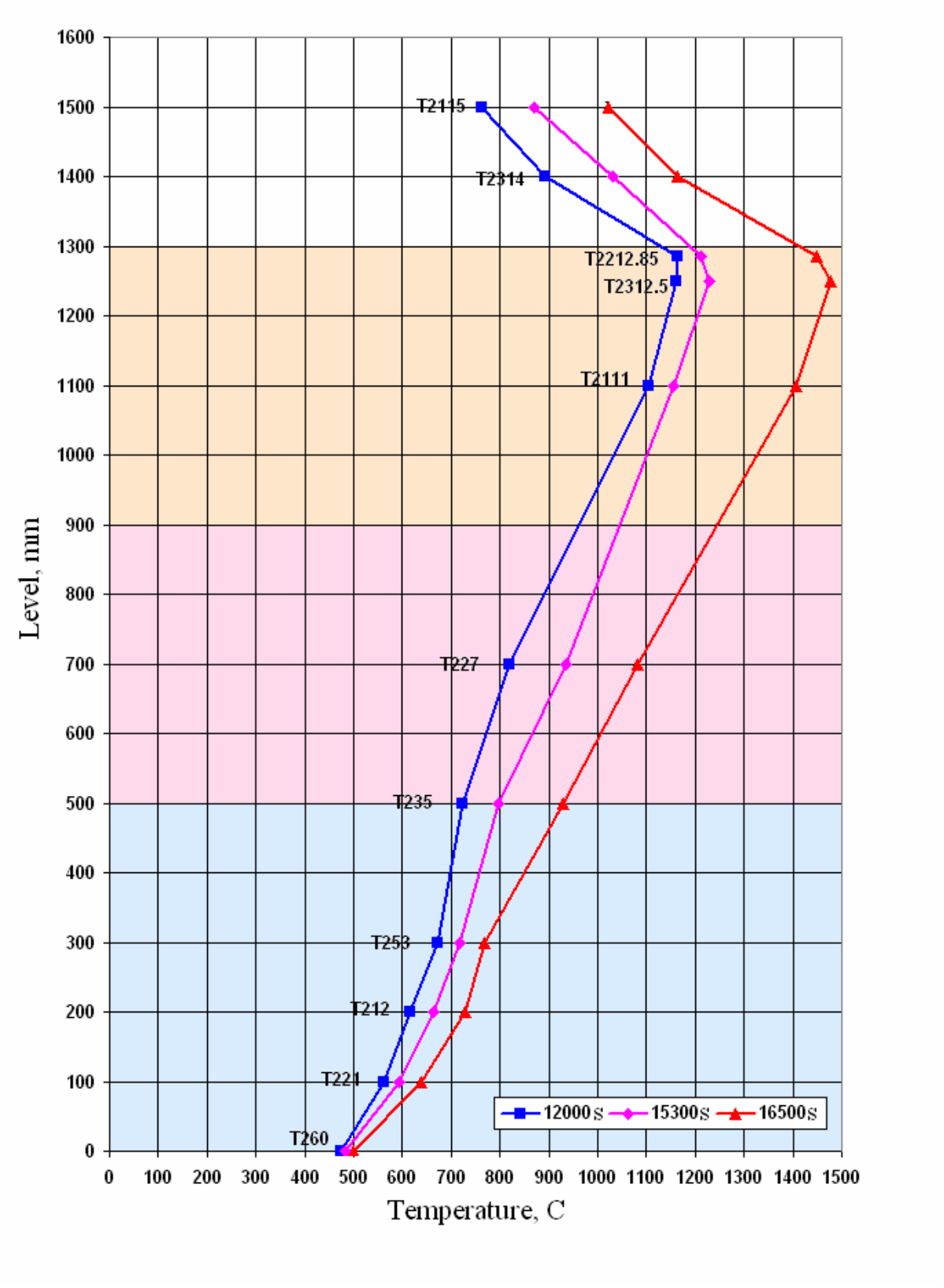

b)

Fig. 1. a – indications of thermocouples fixed on fuel rod claddings at Z = (1100 – 1300) mm elevations of the model FA; b – claddings temperature in the second row over heated zone at the beginning of pre-oxidation (t=12000 s), at the beginning of the transient stage (t=15300 s) and before flooding onset (t=16500 s).

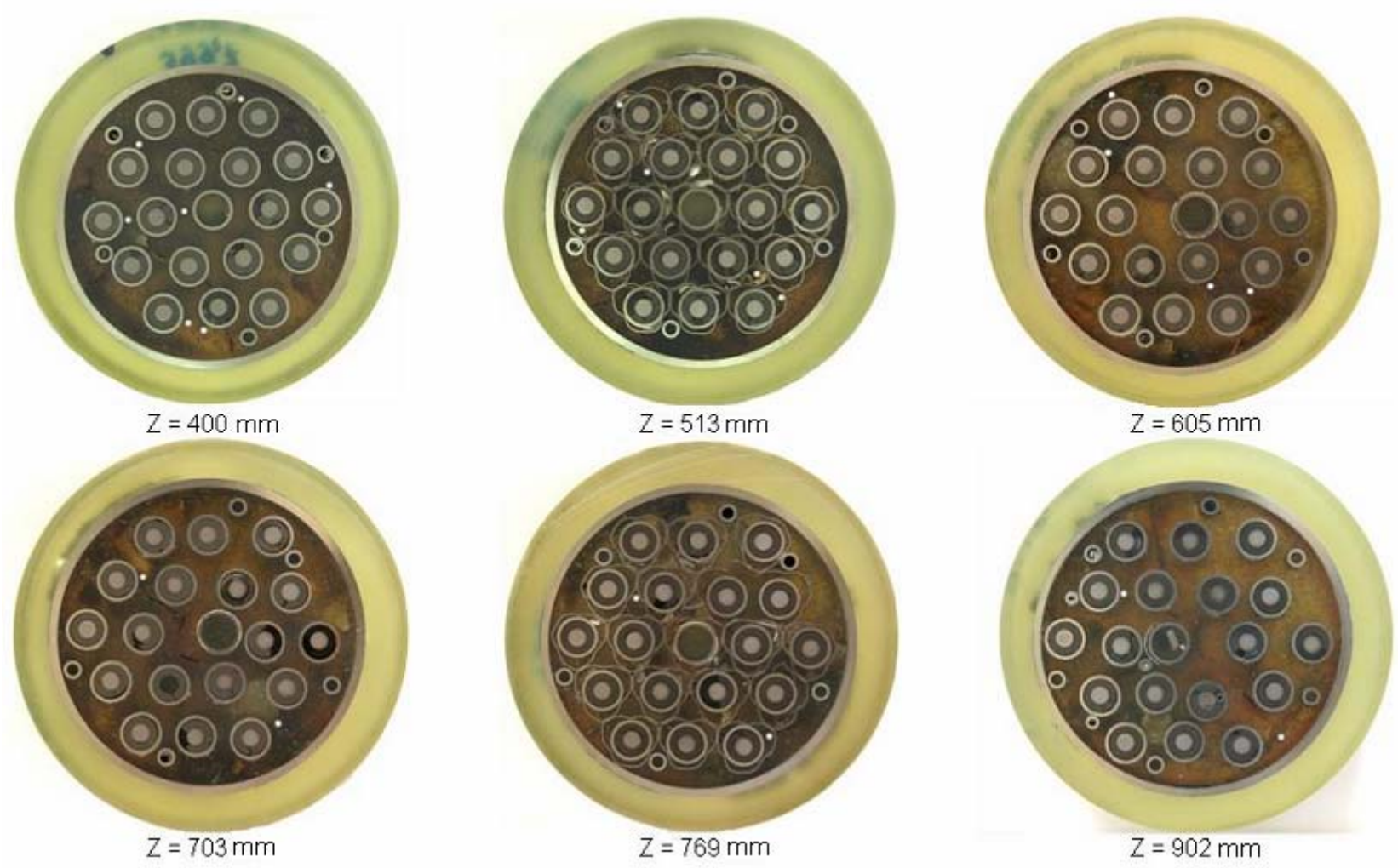

Fig. 2. Photos of the assembly cross-sections slabs within the elevations of Z ~ 400…900 mm.

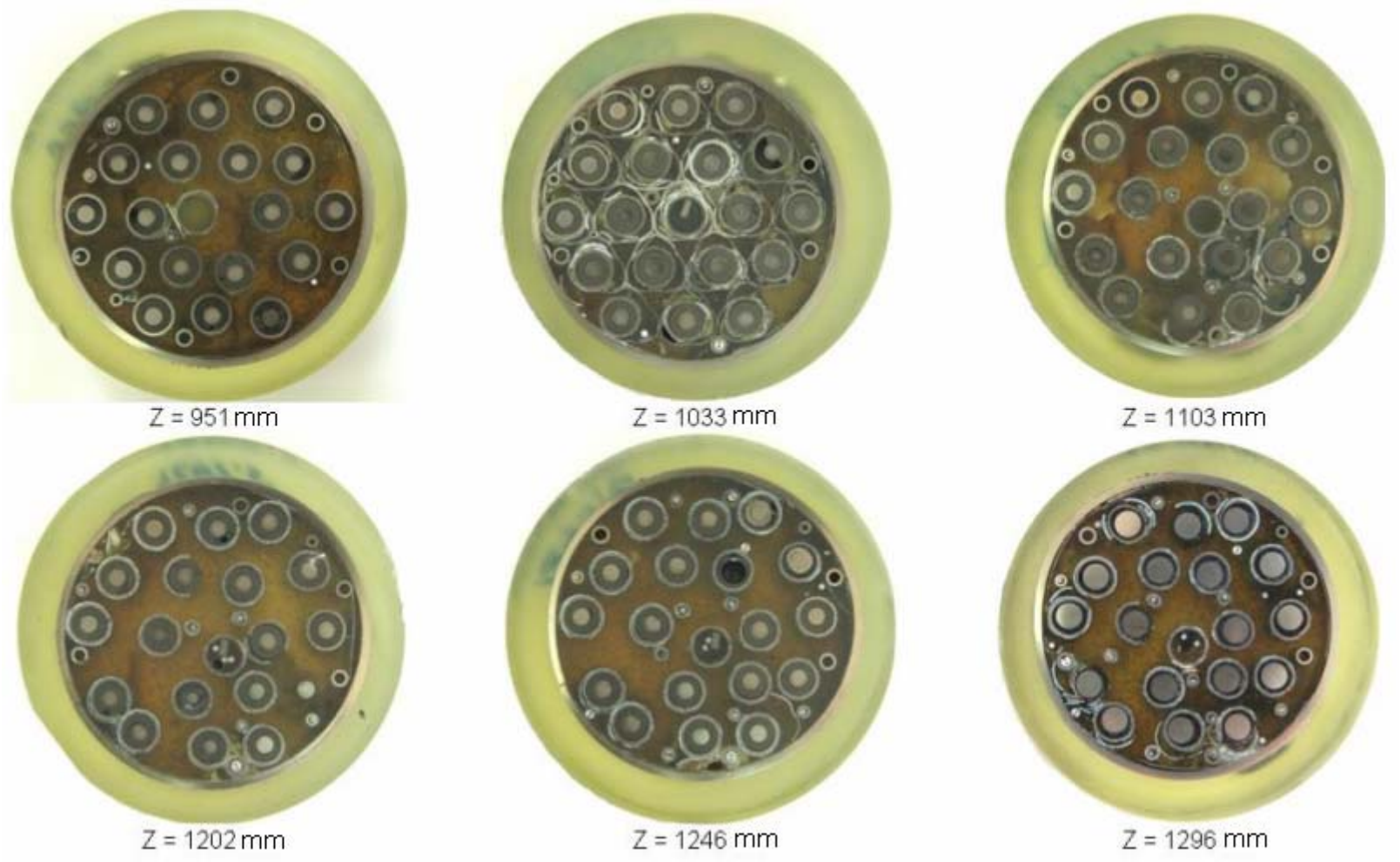

Fig. 3. Photos of the assembly cross-sections slabs within the elevations of Z ~ 950…1300 mm.

a

b

Fig. 4. Post-test appearance of the shroud of the model FA SF2:
a – elevations of Z = 850 - 1050 mm; b – elevations of Z = 1100 - 1300 mm.

Fig. 5. Assembly cross-section at Z = 513 mm elevation (top view).

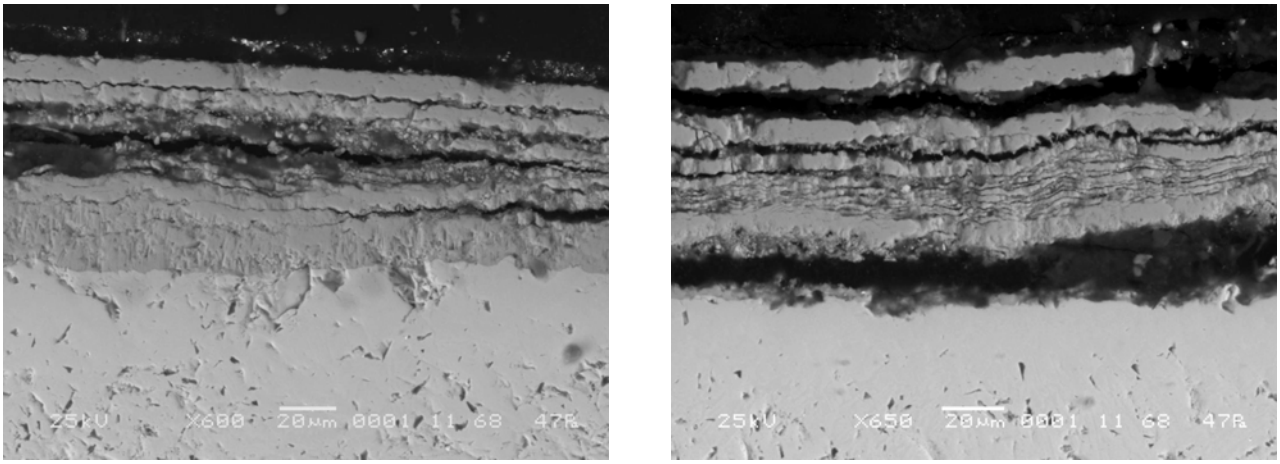

a b

Fig. 6. State of oxide scale on fuel rod claddings surface at Z = 513 mm elevation: a – fuel rod 2.4; b – fuel rod 2.6.

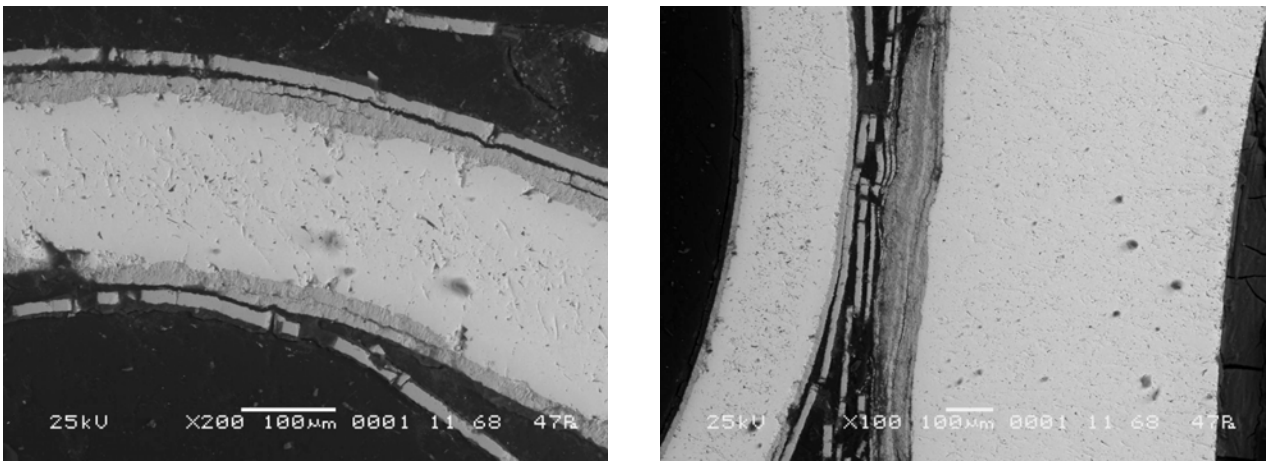

a b

Fig. 7. State of oxide scale on surface of spacer grids and fuel rod claddings at Z = 513 mm elevation: a – cell of fuel rod 2.1; b – fuel rod 1.1.

Fuel rod No.	**1.1**	**2.1**	**2.2**	**2.3**	**2.4**	**2.5**	**2.6**
Metal layer thickness, μm	611	647	643	656	644	630	627
Fuel rod No.	**3.1**	**3.2**	**3.3**	**3.4**	**3.5**	**3.6**	**3.7**
Metal layer thickness, μm	629	652	661	659	661	666	662
Fuel rod No.	**3.8**	**3.9**	**3.10**	**3.11**	**3.12**		
Metal layer thickness, μm	659	656	642	628	623		

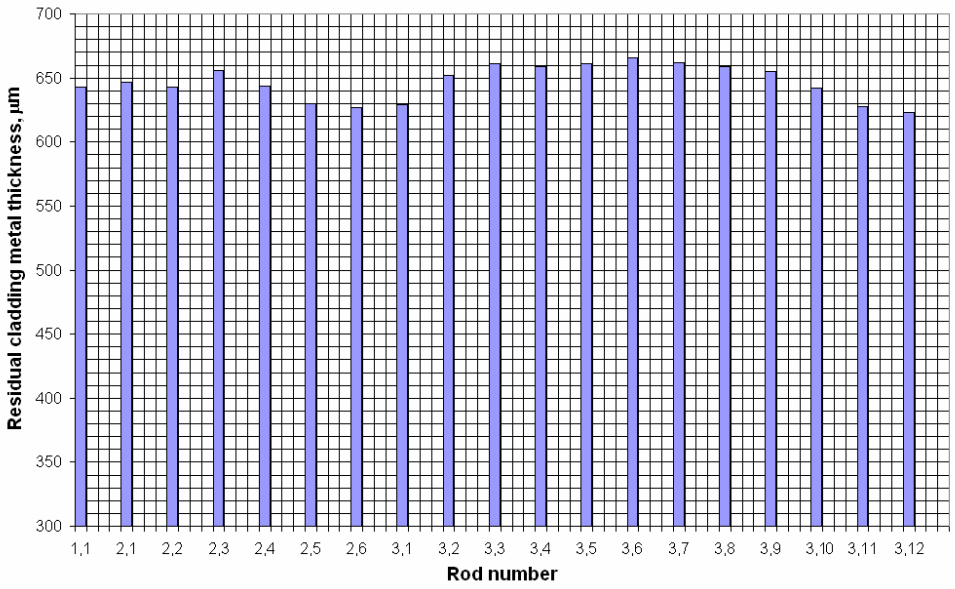

Fig. 8. Results of thickness measurement of claddings metal layer at Z = 513 mm elevation.

Fig. 9. Assembly cross-section at Z = 702 mm elevation (top view).

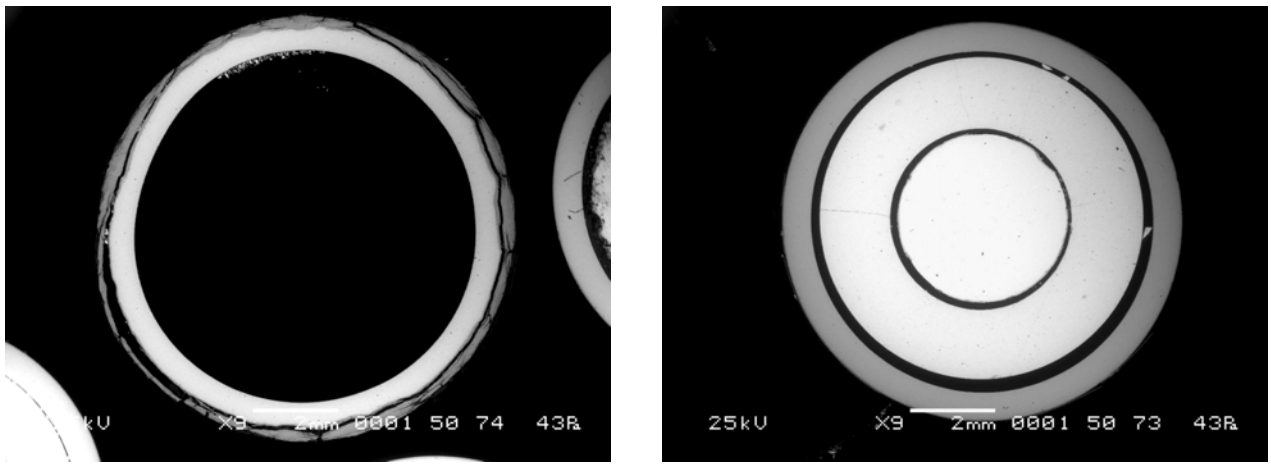

a b

Fig. 10. Cross-section of fuel rod simulators:
a – fuel rod 1.1; b – fuel rod 2.4 at Z = 702 mm elevation.

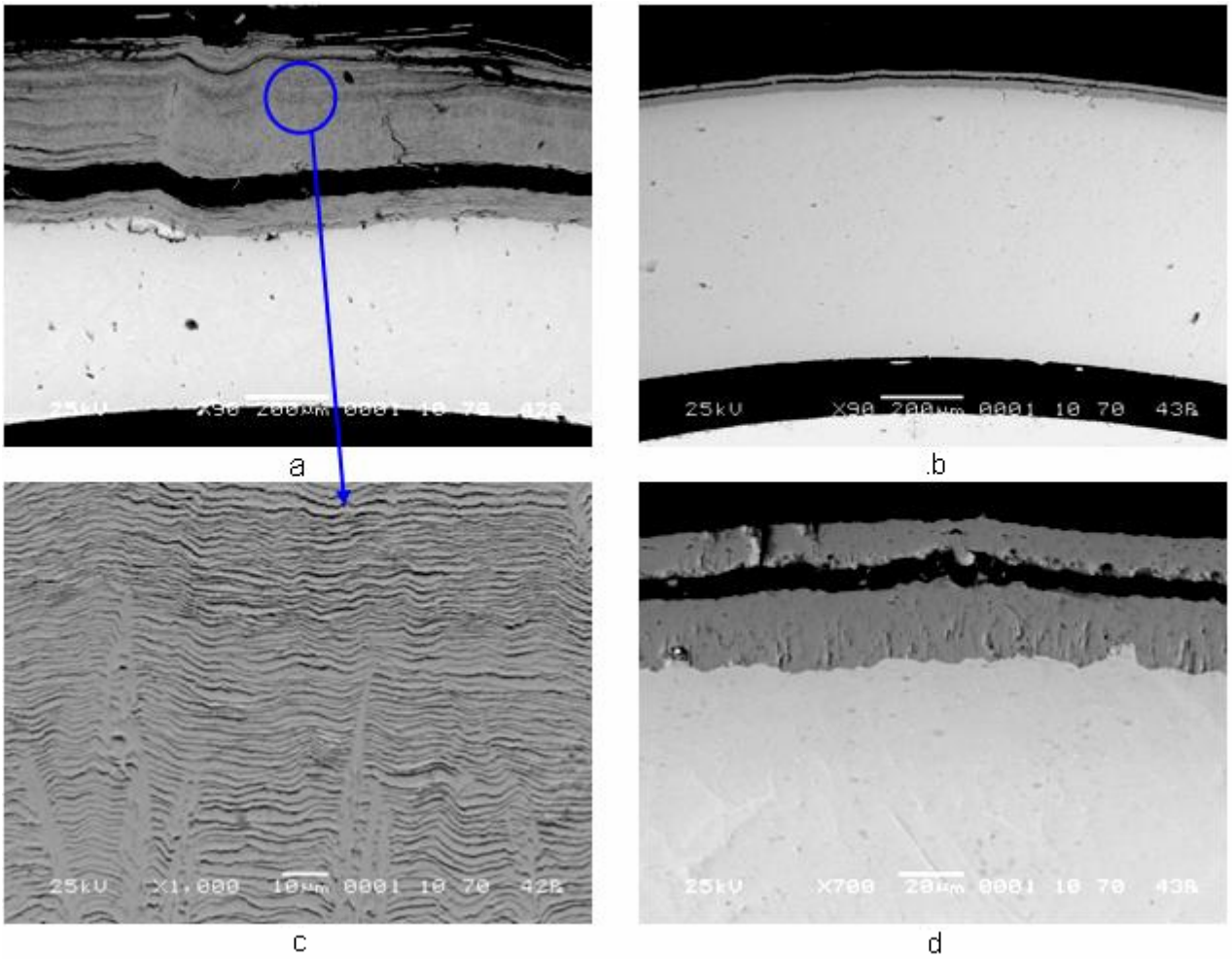

Fig. 11. State of fuel rod simulator claddings (a – fuel rod 1.1; b – fuel rod 2.4) and their oxide scales (c – multilayered oxide scale on surface of cladding of fuel rod 1.1; d – typical oxidation state of the other fuel rods claddings) at Z = 702 mm elevation.

Fuel rod No.	1.1	2.1	2.2	2.3	2.4	2.5	2.6
Metal layer thickness, μm	510	647	653	655	647	651	630
Fuel rod No.	3.1	3.2	3.3	3.4	3.5	3.6	3.7
Metal layer thickness, μm	631	657	662	657	641	643	656
Fuel rod No.	3.8	3.9	3.10	3.11	3.12		
Metal layer thickness, μm	659	656	641	640	649		

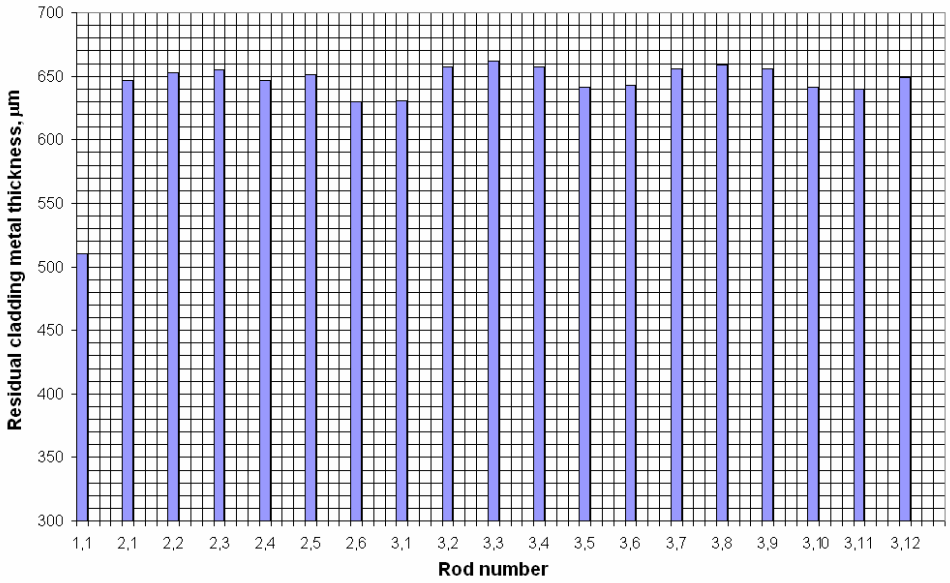

Fig. 12. Results of thickness measurement of claddings metal layer at Z = 702 mm elevation.

Fig. 13. Assembly cross-section at Z = 1033 mm elevation (top view).

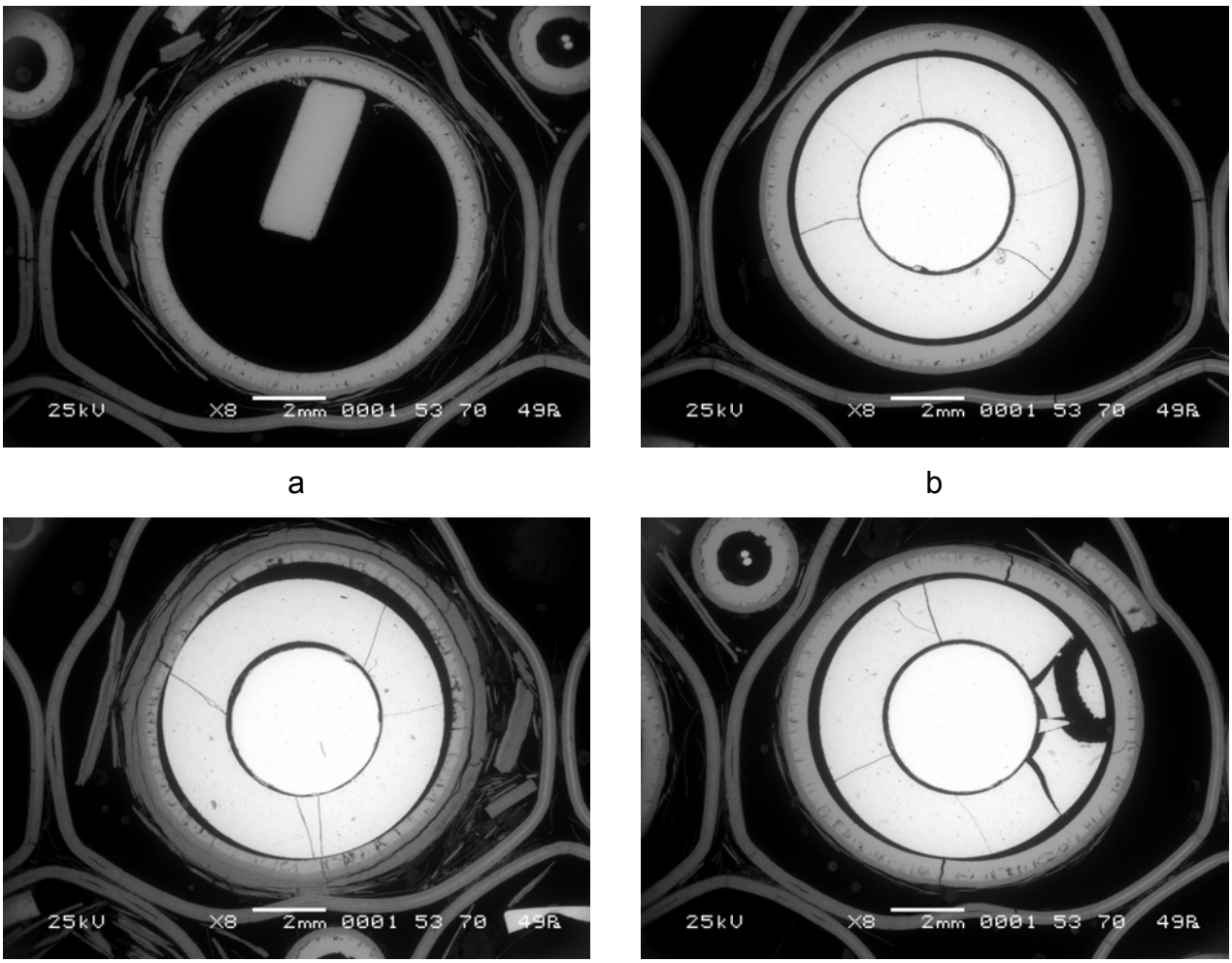

Fig. 14. Cross-section of fuel rod simulators: a – fuel rod 1.1; b – fuel rod 2.2; c – fuel rod 2.5; d – fuel rod 2.6 at Z = 1033 mm elevation.

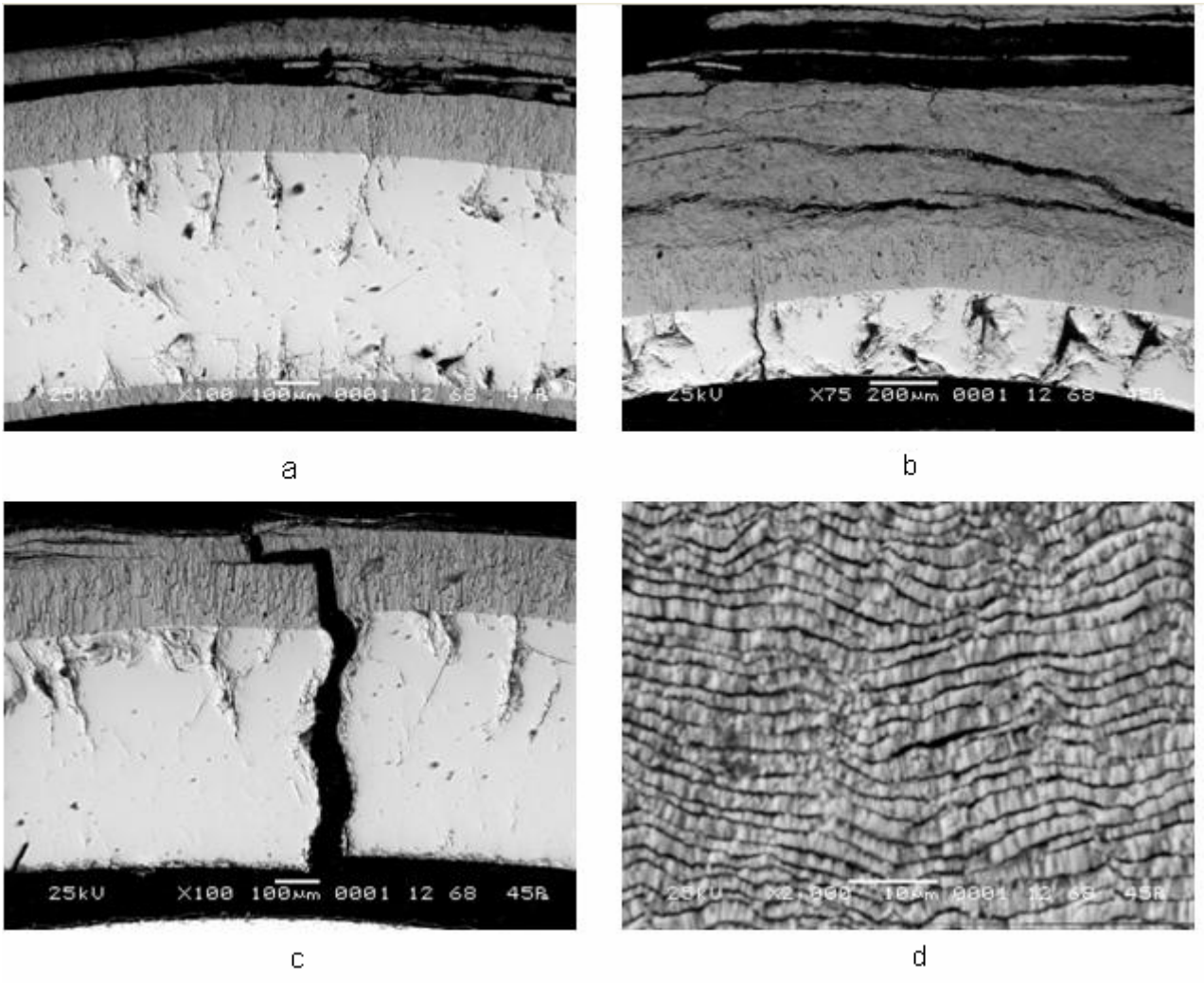

Fig. 15. State of fuel rod simulator claddings (a – fuel rod 1.1; b – fuel rod 2.5) and oxide scales (c – oxide scale on surface of cladding of fuel rod 2.6; d – multilayered oxide on surface of cladding of fuel rod 2.5) at Z = 1033 mm elevation.

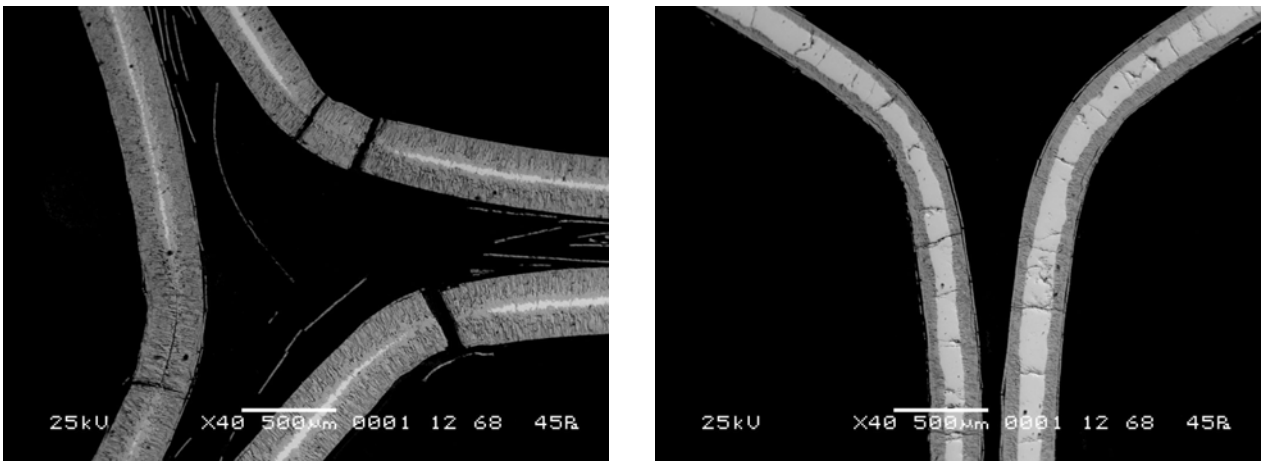

Fig. 16. State of spacer grid at Z = 1033 mm elevation: a – area of the second row of fuel rods; b – area of the third row of fuel rods.

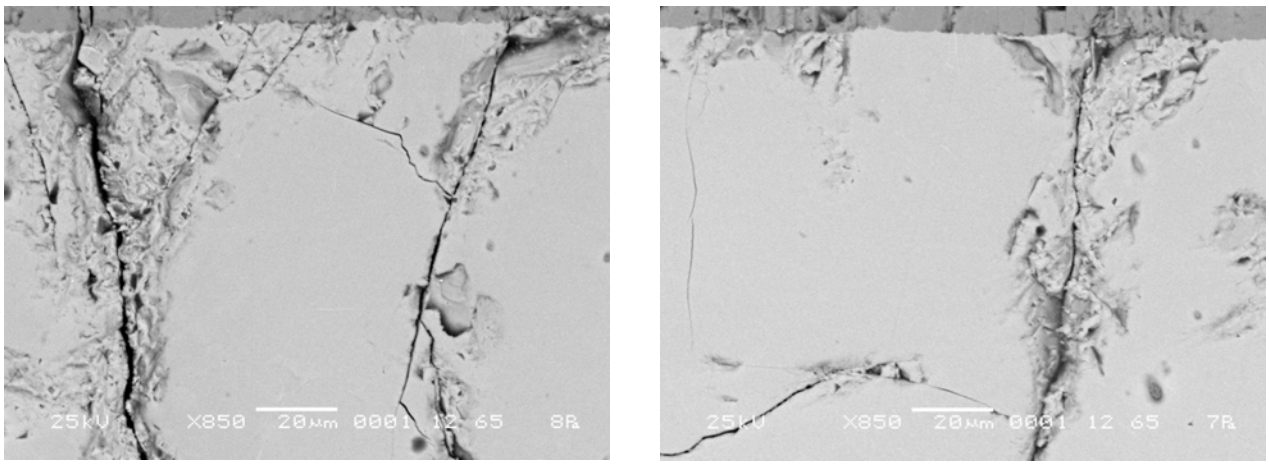

a b

Fig. 17. State of cracks in fuel rod claddings at Z = 1033 mm elevation:
a – fuel rod 2.4; b – fuel rod 3.12.

Fuel rod No.	**1.1**	**2.1**	**2.2**	**2.3**	**2.4**	**2.5**	**2.6**
Metal layer thickness, μm	491	537	547	533	560	310	509
Fuel rod No.	**3.1**	**3.2**	**3.3**	**3.4**	**3.5**	**3.6**	**3.7**
Metal layer thickness, μm	532	525	596	594	540	556	602
Fuel rod No.	**3.8**	**3.9**	**3.10**	**3.11**	**3.12**		
Metal layer thickness, μm	590	599	582	570	533		

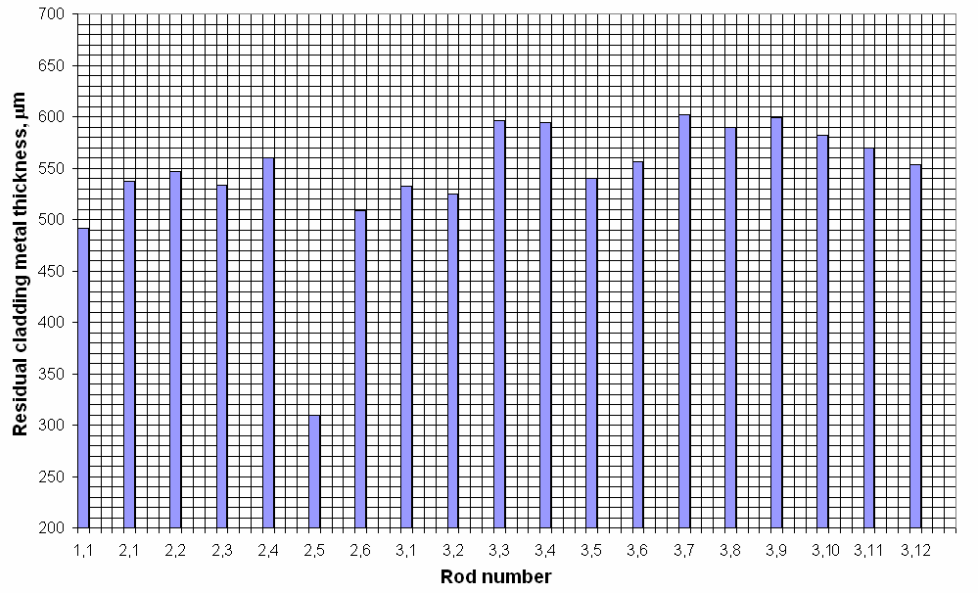

Fig. 18 Results of thickness measurement of claddings metal layer at Z = 1033 mm elevation.

Fig. 19. Assembly cross-section at Z = 1103 mm elevation (top view).

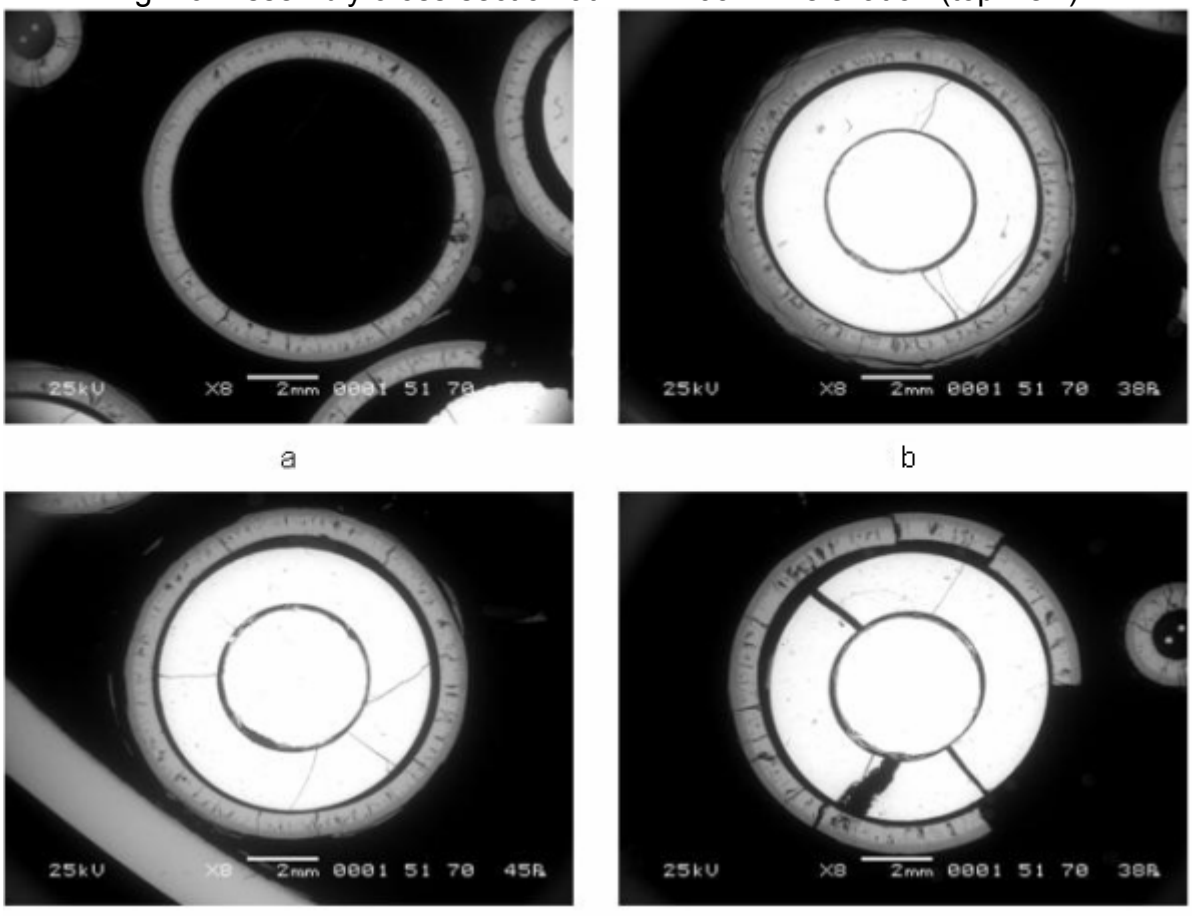

Fig. 20. Cross-section of fuel rod simulators (a - fuel rod 1.1; b – fuel rod 2.2; c – fuel rod 3.3; d – fuel rod 2.3) at Z = 1103 mm elevation.

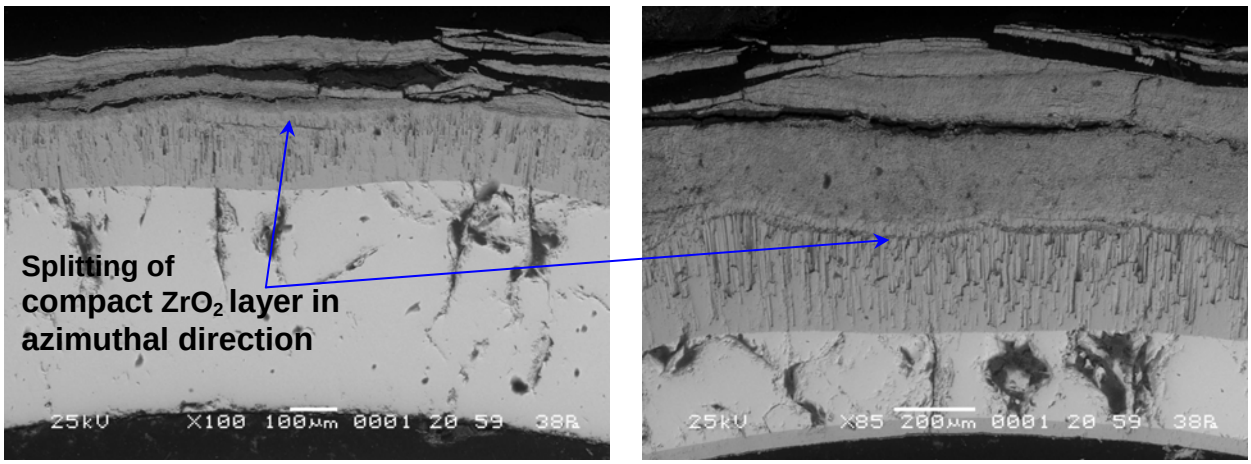

a b

Fig. 21. State of oxide scale on the surface of fuel rod claddings (a – cladding of fuel rod 2.5; b – cladding of fuel rod 2.2) at Z = 1103 mm elevation.

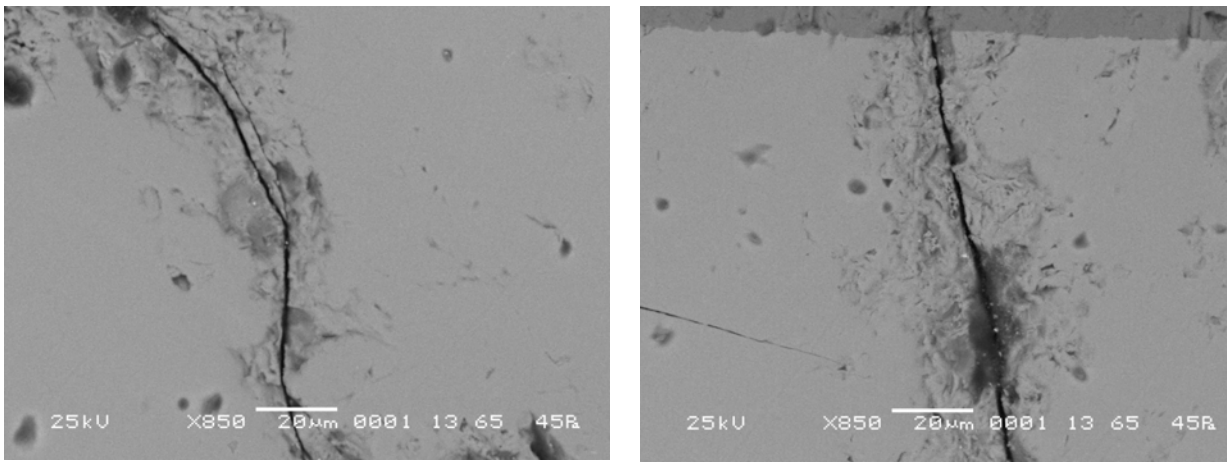

a b

Fig. 22. State of cracks in fuel rod claddings at Z = 1103 mm elevation: a – fuel rod 2.1; b – fuel rod 3.11.

Fuel rod No.	1.1	2.1	2.2	2.3	2.4	2.5	2.6
Metal layer thickness, μm	484	469	308	497	518	470	508
Fuel rod No.	3.1	3.2	3.3	3.4	3.5	3.6	3.7
Metal layer thickness, μm	544	0	489	511	409	512	547
Fuel rod No.	3.8	3.9	3.10	3.11	3.12		
Metal layer thickness, μm	601	568	548	585	537		

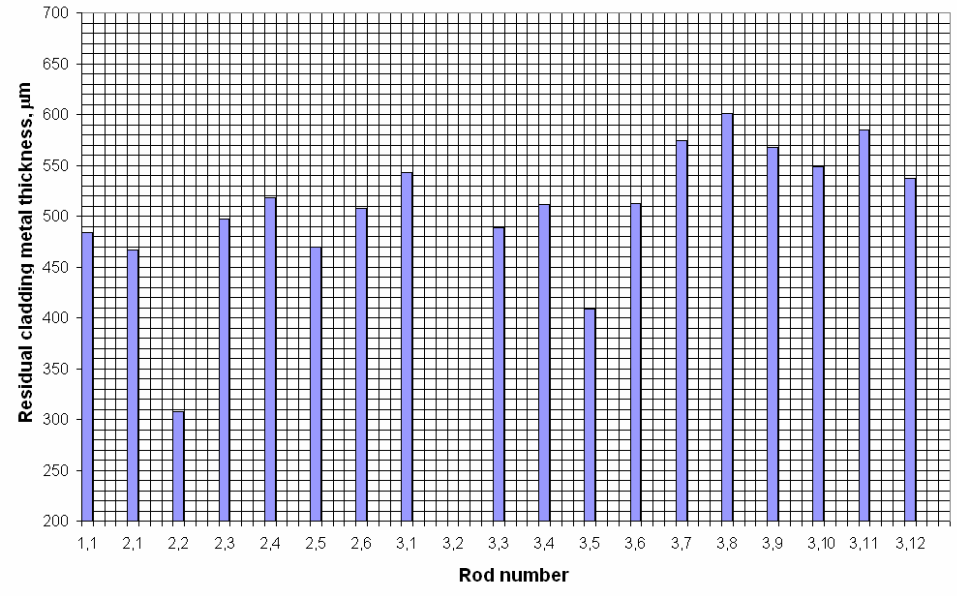

Fig. 23. Results of thickness measurement of claddings metal layer at Z = 1103 mm elevation.

Fig. 24. Assembly cross-section at Z = 1250 mm elevation (top view).

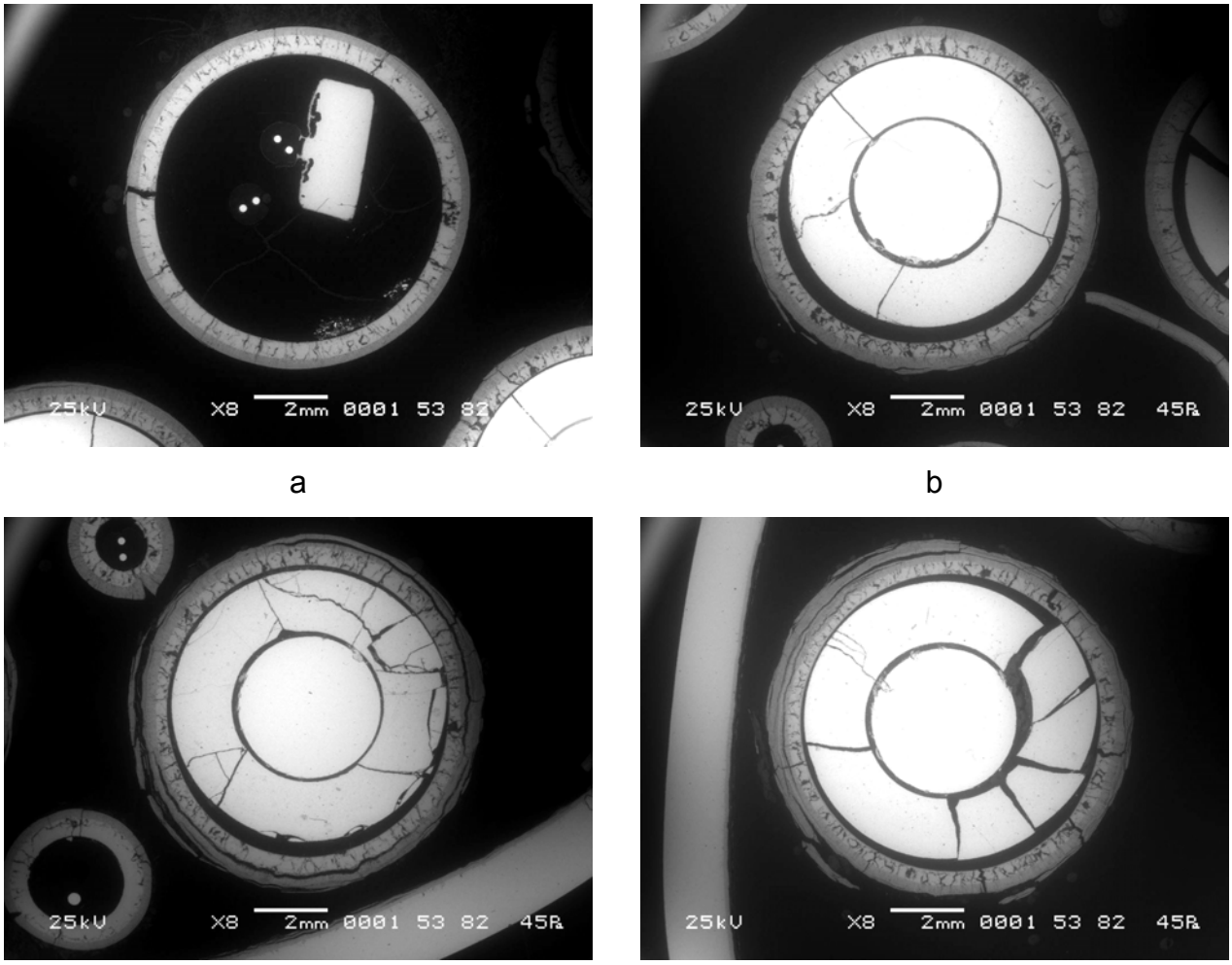

a b

c d

Fig. 25. Cross-section of fuel rod simulators (a – fuel rod 1.1; b – fuel rod 2.1; c – fuel rod 3.1; d – fuel rod 3.5) at Z = 1250 mm elevation.

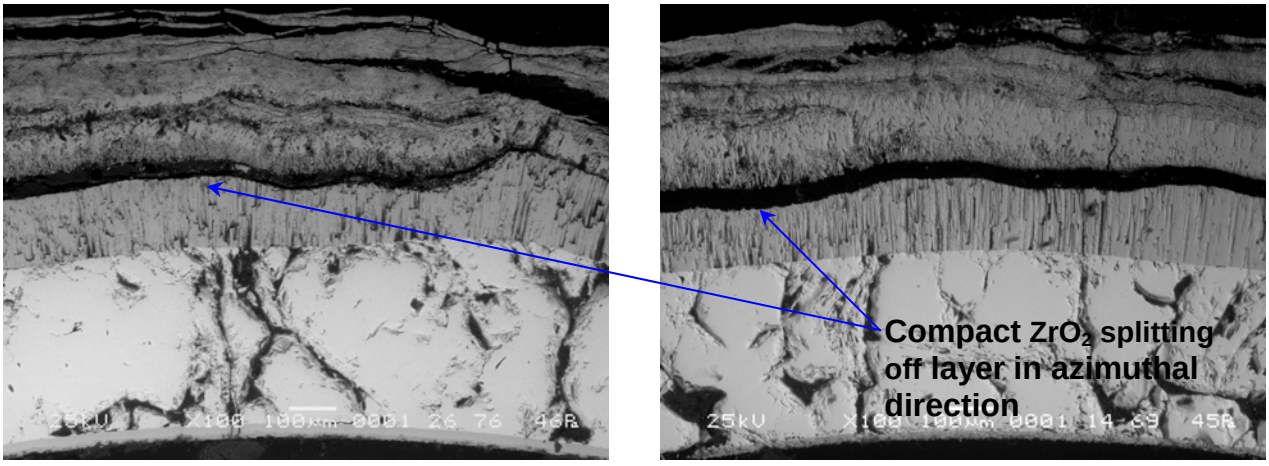

a b

Fig. 26. State of oxide scale on surface of fuel rod claddings (a – cladding of fuel rod 2.4; b – cladding of fuel rod 2.3) at Z = 1250 mm elevation.

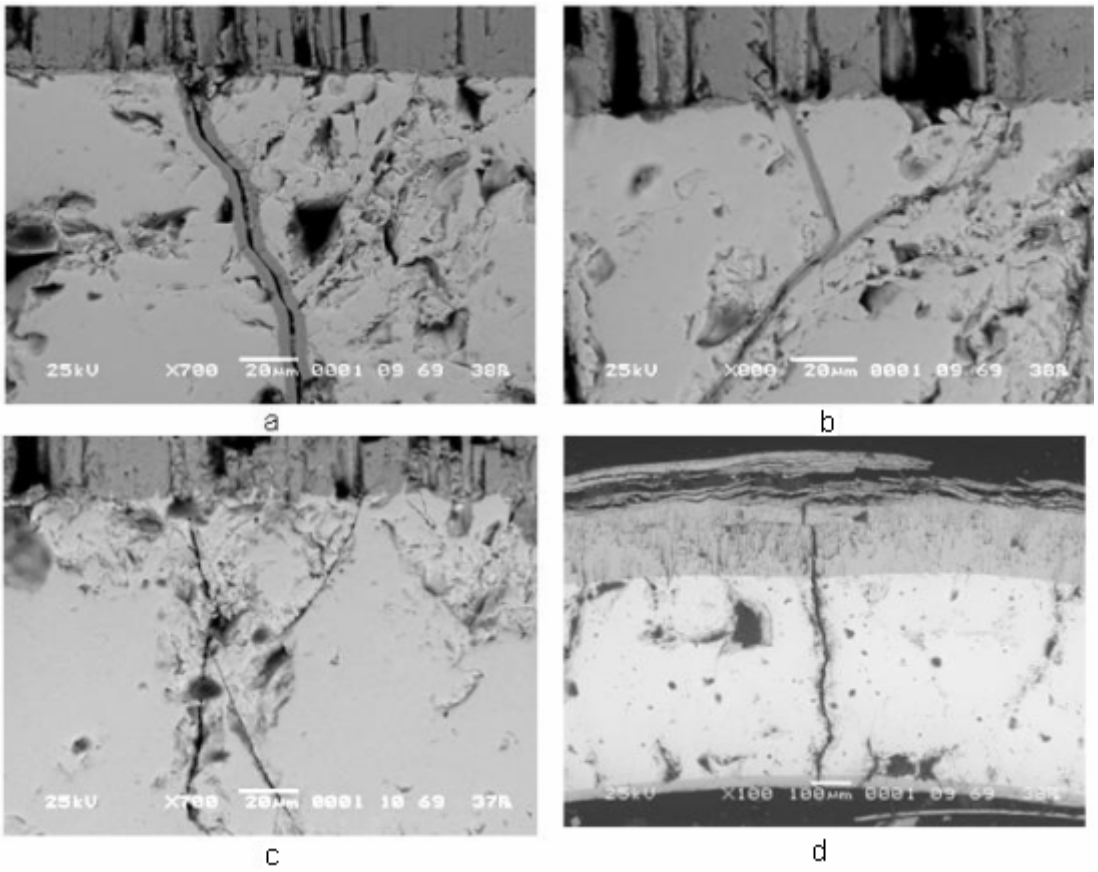

Fig. 27. State of cracks in fuel rod claddings at Z = 1250 mm elevation:
a, b – fuel rod 3.12; c, d – fuel rod 2.4.

Fuel rod No.	**1.1**	**2.1**	**2.2**	**2.3**	**2.4**	**2.5**	**2.6**
Metal layer thickness, μm	507	415	387	388	444	434	448
Fuel rod No.	**3.1**	**3.2**	**3.3**	**3.4**	**3.5**	**3.6**	**3.7**
Metal layer thickness, μm	362	359	286	310	259	353	384
Fuel rod No.	**3.8**	**3.9**	**3.10**	**3.11**	**3.12**		
Metal layer thickness, μm	382	308	393	513	465		

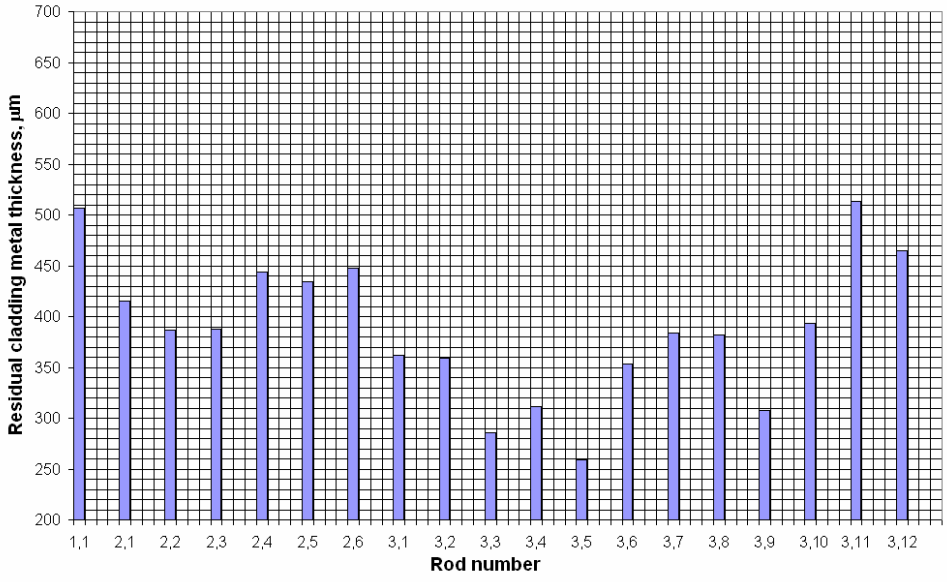

Fig. 28. Results of thickness measurement of claddings metal layer
at Z = 1250 mm elevation.

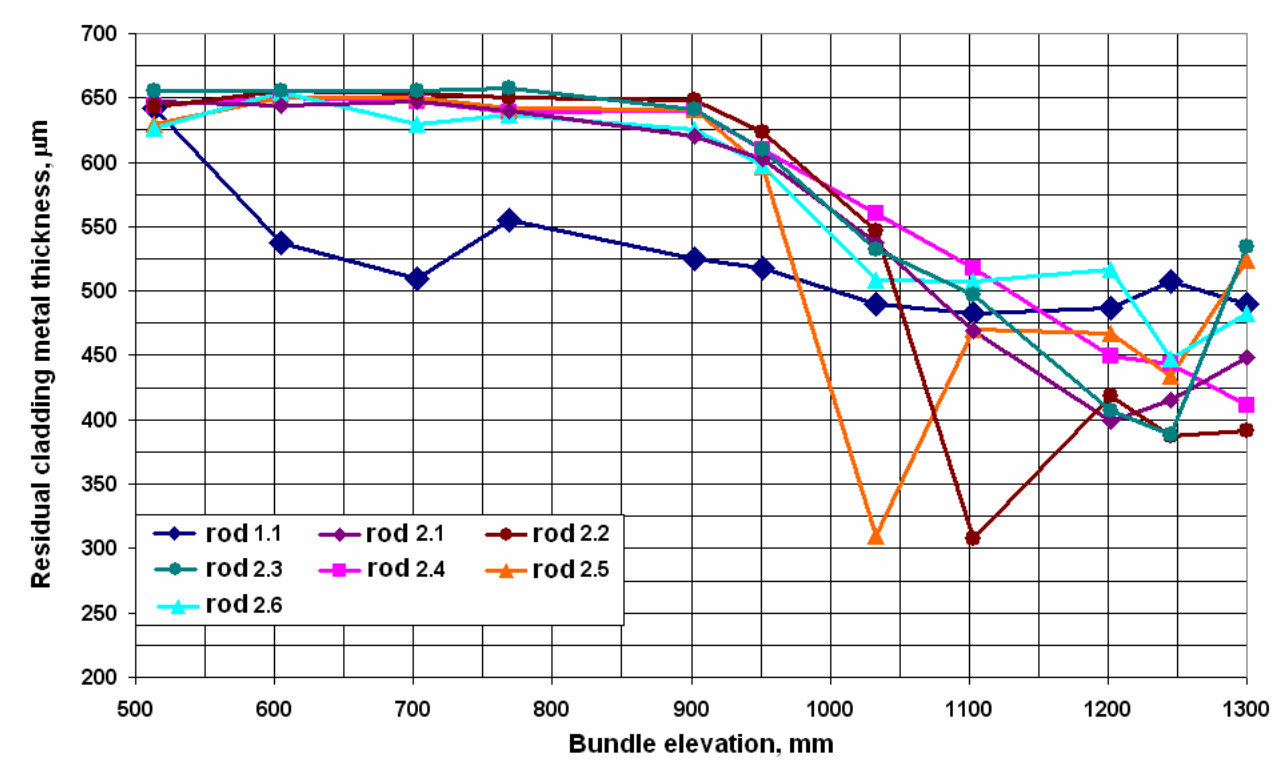

Fig. 29. Distribution of thickness of the remained metal part of claddings of fuel rods in the second row over heated zone.

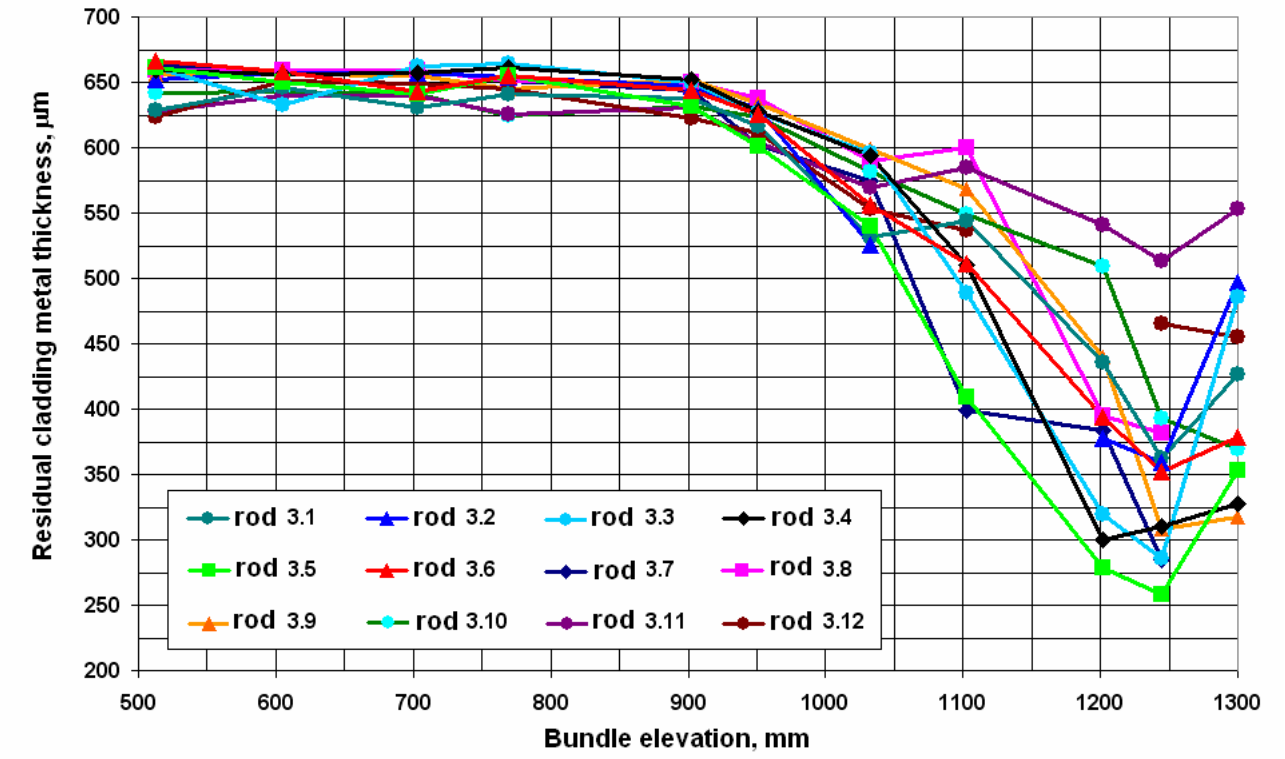

Fig. 30. Distribution of thickness of the remained metal part of claddings of fuel rods in the third row over heated zone.

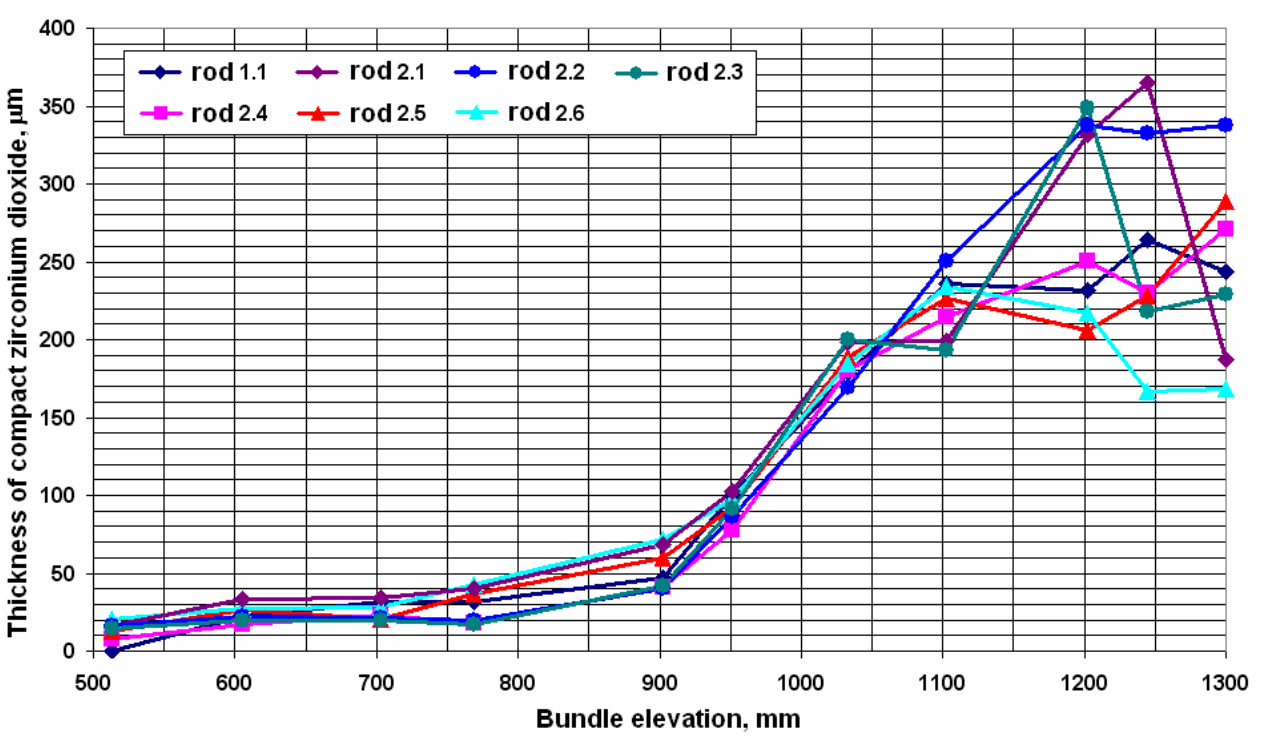

Fig. 31. Distribution of thickness of the compact ZrO_2 layer on external surface of fuel rods in the second row over heated zone.

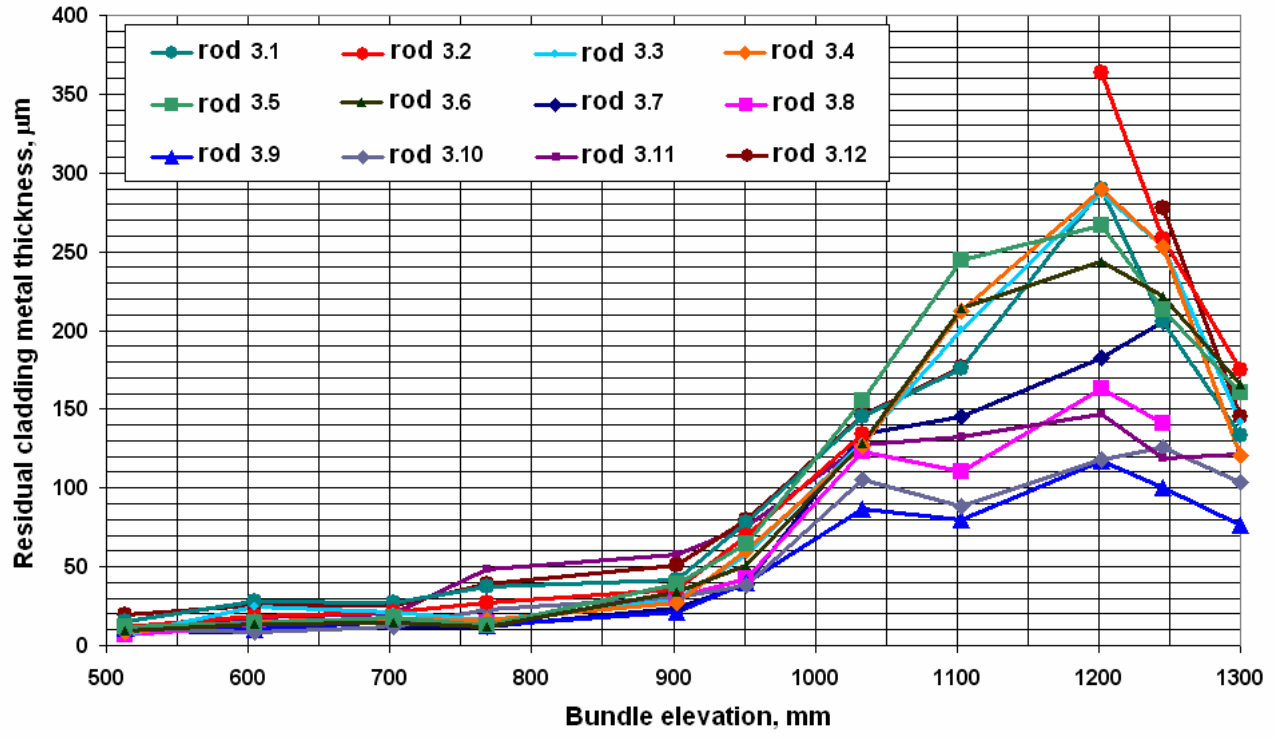

Fig. 32. Distribution of thickness of the compact ZrO_2 layer on external surface of fuel rods in the third row over heated zone.

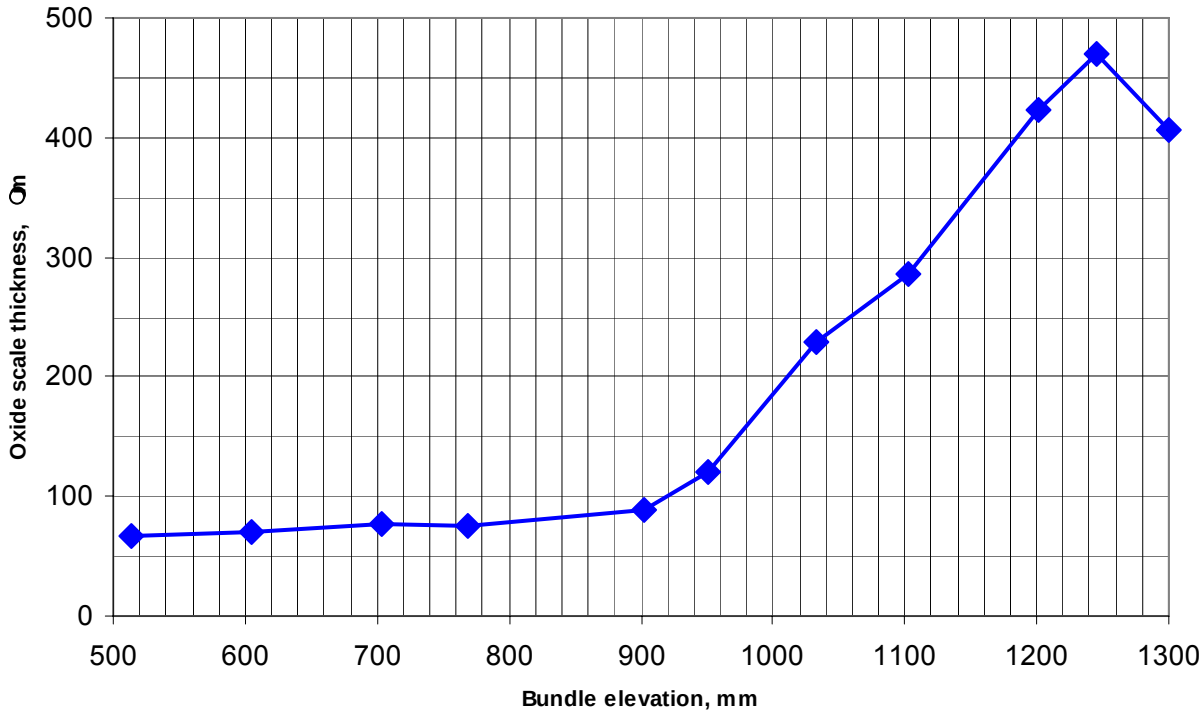

Fig. 33. Distribution of the averaged calculated ZrO_2 thickness on external surface of fuel rods claddings in the second and third rows over heated zone.